uOttawa

Department of Mechanical Engineering
Faculty of Engineering
University of Ottawa

The Dynamic Response of Enteric Neurons to Polymeric Substrates

Author: Dilara Jakupovic
Supervisor: Dr. Fabio Variola

Thesis submitted to the University of Ottawa
in partial fulfillment of the requirements for the
MASc in Biomedical Engineering

Abstract

The enteric nervous system (ENS) is commonly referred to as the 'second brain' due to its complex networks of neuronal cells. The abnormality of these neurons and/or their absence has been shown to play a fundamental role in diseases of both the ENS and the central nervous system. Accordingly, electrophysiological studies of the ENS and general understanding of how enteric neurons behave in the gastrointestinal tract are critical in the characterization of the pathophysiology of enteric and neurodevelopmental diseases. To date, studies on these aspects have been limited by the difficulty of culturing enteric neurons *in-vitro*, as well as by their poor adhesion properties. The primary objectives of this thesis are to develop strategies to investigate electrodynamics processes of enteric neurons and close in on their interactions with polymeric substrates, aiming at optimizing conventional experimental approaches and expanding the current knowledge and critical understanding of this elusive cell type.

By capitalizing on a rapid and efficient culturing method developed by our group, different polymers were tested in order to assess their ability to promote adhesion of enteric neurons, as confirmed by immunofluorescence analysis. The most effective polymer resulting from this initial screening was then applied as a coating onto the glass surface of multichannel electrode arrays (MEAs) allowing for the analysis of neuron dynamics. While Matrigel® was the most effective at promoting both neuron adhesion and neurite outgrowth, it acted as an insulating material which prevented the MEA electrodes from picking up electrical signals. Therefore, we opted instead for laminin protein and poly-d-lysine immobilized on glass by polydopamine, to study the electrophysiology of the neurons. Of note, polydopamine was found to be critical in enhancing the stability of the protein coating and ensuring cellular viability.

The same protein coating was also used to functionalize the surface of blends of poly(styrene) and poly(methyl methacrylate), which segregate when mixed to give rise to varying topographical features. These surfaces aimed at elucidating fundamental processes that dictate how neurons interact with surfaces when compared to smooth rigid surfaces (i.e. glass).

Finally, the most effective surface for neuron adhesion was applied to study how chemotaxis influences neurite elongation and directionality. Enteric neurons were cultured onto both a linear concentration gradient of protein created using a microfluidic system and a uniform concentration profile to compare their response to chemical signals. In general, their motion was random and lacked directionality on the uniform protein surface. The neuronal response to the chemical gradient could not be evaluated to completion; however, this analysis still provided meaningful insight as a starting point for future studies.

The results presented in this thesis serve as a significant stepping-stone for the improvement of the *in-vitro* study of the ENS and will be used to gain a deeper understanding of enteric diseases, ultimately contributing to the development of novel polymeric scaffolds for tissue-engineering applications.

Acknowledgments

I would like to express my gratitude to my supervisor Dr. Fabio Variola for his guidance and support over the course of my Masters. I am also thankful for the help of Alexander Steeves for all of the microscopy and AFM work performed towards this work.

I would also like to acknowledge the technicians and staff at the University of Ottawa who offered their time and knowledge to teach me new techniques and enable me to complete my thesis, including Skye McBride and Dr. Chloe van Oostende-Triple for helping to troubleshoot my cellular imaging and Yun Liu for her SEM characterization expertise.

My sincere gratitude is given to Dr. Elena Martinez for the hospitality and support during my stay at the Institute for Bioengineering of Catalonia (IBEC) in Barcelona. *Muchas gracias* to the entire Biomimetic Systems for Cell Engineering Group, and especially to Enara Larrañaga for taking me under her wing and teaching me how to create chemical gradients.

Finally, I owe gratitude to Dr. Sarah Schock, without whom this work would not have been possible. Thank you for your knowledge and support. I am also thankful to Dr. William Staines for sharing his laboratory space and love of neuroscience, and to Kristen Deloughery for all of her help in the lab.

The work in this thesis was supported by the Canada Foundation for Innovation (CFI), the Natural Sciences and Engineering Research Council of Canada (NSERC), and the Children's Hospital of Eastern Ontario (CHEO).

Table of Contents

Lists of Figures

List of Tables

Nomenclature

AFM	Atomic force microscopy
$CaCl_2$	Calcium chloride
Ch	Chitosan
CNS	Central nervous system
DAPI	4',6-Diamidino-2-phenylindole
DMEM	Dulbecco's modified Eagle medium
ECM	Extracellular matrix
EN	Enteric neuron
ENS	Enteric nervous system
FTIR	Fourier transform infrared spectroscopy
Gp	Genipin
HBSS	Hank's balanced salt solution
HEPES	4-(2-Hydroxyethyl)-1-piperazineethanesulfonic acid
KCl	Potassium chloride
LMMP	Longitudinal muscle and myenteric plexus
PDA	Polydopamine
PDL	Poly-d-laminin
PMMA	Poly(methyl methacrylate)
PS	Poly(styrene)
MEA	Microelectrode array
$MgCl_2$	Magnesium chloride
MP	Myenteric plexus
MW	Molecular weight
NaCl	Sodium chloride
$NaHCO_3$	Sodium bicarbonate
Na_2HPO_4	Disodium phosphate
PBS	Phosphate buffered saline
SEM	Scanning electron microscopy

Chapter 1- Introduction

1.1 Motivation

The enteric nervous system (ENS) is a partly autonomous part of the body's nervous system that comprises the gastro-intestinal tract and is responsible for regulating endocrine and immune functions [1, 2]. It is the largest component of the peripheral nervous system and is often referred to as the 'second brain' due to its complex networks of more than fifteen neuronal cell types and integrated circuits [3–5]. In addition, the 100 million neurons comprising the ENS are able to operate independently of the central nervous system [6, 7].

Neurons are found within the ENS in one of two major neuronal plexuses, namely the myenteric (MP) and the submucosal (SMP). It is within these that they respond to various physiochemical stimuli with coordinated refluxes like muscle contraction, allowing them to manage processes within the gastro-intestinal system. These processes include, but are not limited to, regulating fluid flow, absorption of nutrients, and initiating immune responses [2].

The activity of the ENS is critical to normal body functions, and accordingly, damage to the system raises the potential for serious to life threatening consequences [8]. Hirschsprung's disease, a congenital disorder, is characterized by the absence of enteric neurons in the distal bowel and if left undiagnosed at birth, can become fatal [2, 8]. Similarly, changes in ENS neuropathology has been shown to manifest into incontinence, inflammatory bowel disease, and gastroenteropathy in diabetes mellitus [4, 9, 10]. Increasingly, it is also being shown that the ENS plays a role in disorders of the central nervous system such as Parkinson's and Alzheimer's, as well as in neurodevelopmental diseases such as autism and Rett's disease [11–14]. Despite the ENS being critical to the normal functioning of the gut and playing a part in other disorders, it continues to remain elusive.

In the last decade, a large body of literature has focused on neurochemistry and neuronal engineering through the development of custom-made nanotopographical substrates to elucidate cortical neuronal behavior. In this context, nanotopograhy has shown the distinct ability to influence neuron adhesion and guide neurite and axon development and alignment [15, 16]. However, despite such progress in the investigation of cortical neurons, equivalent studies focused on enteric neurons are lagging behind, mostly due to the problems associated with EN isolation and culturing. Similarly, research in the field of gut health has in fact been limited by the paucity of data available regarding the development of gut neuron motility, stemming from the difficulty of culturing enteric neurons *in-vitro* [7, 11]. Therefore, it is necessary to develop improved methods for the study of enteric neurons to be able to understand the physiology behind the various manifestations of gastrointestinal diseases and their symptoms [17].

1.2 Main Objectives

To bridge this gap, this Thesis provides strategies and experimental tools to enable enteric neuron-based studies aimed at investigating their electrodynamic properties and elucidating the complex phenomena that drive how enteric neurons sense and respond to nanoengineered substrates. Results from this study promise to generate new knowledge of both fundamental and practical importance by providing the key to unlock aspects of neuronal development and advance practical applications, such as multi-electrode arrays and neuro-regenerative medicine.

In particular, this thesis outlines experimental data and analysis with the primary goals of developing and optimizing strategies and techniques to isolate, culture, and study enteric neurons towards a better understanding of how they interact with custom-made substrates. To achieve this, the focused goals of this work are to:

1. Screen and evaluate substrates capable of enabling the study of enteric neuron electrophysiology on microelectrode arrays (MEAs) **(Objective 1)**
2. Study the effects of nanotopography on enteric neuron behavior **(Objective 2)**
3. Examine how enteric neuron development is impacted by surface chemistry by using chemical gradients **(Objective 3)**

1.3 Relevance

Very few research groups worldwide have been able to consistently culture enteric neurons and there are limited reports of success measuring EN electrophysiology using microelectrode readers. However, as the enteric nervous system is a critical player in the development of neurological and physiological disorders in both children and adults, it is of great importance to gain a better understanding of the fundamental properties of enteric neurons and the interactions with their *in-vivo* environment. Findings from the experiments presented will serve as a starting point for the development of treatment systems in gastrointestinal disorders.

1.4 Enteric Neurons

The ENS is composed of hundreds of millions of cells, which work in concert to regulate numerous functions within the gastro-intestinal tract including digestion, fluid flow, nutrient absorption, and immune response [1]. It can function autonomously from the central nervous system (CNS), however there remains a chain of signal transduction through the vagus nerve to facilitate communication between the ENS and CNS [18].

There are three main types of neurons within the ENS: primary afferent, motor, or interneurons. Primary afferent neurons, or sensory neurons, are responsible for detecting both chemical and mechanical signals in their environment, while motor neurons accept these signals

and output them to the circular muscle. The communication between these two types is facilitated by interneurons by propagating the signals between them [1].

The ENS presents a unique environment compared to the CNS, as it is regularly exposed to external stimuli, primarily in the form of food. Similarly, the process of digestion requires muscle contraction which introduces a mechanical form of stimulus that is not present in the brain. In addition, the contents of the stomach are acidic, thus there is mucus constantly being secreted to mediate the pH, further diversifying the environment of the ENS and distinguishing it from that of the CNS.

Enteric neurons, more specifically, are found in the extracellular matrix of the ENS which consists of a variety of proteins, including laminin and collagen, and proteogylcans such as fibronectin [19]. While this presents a niche very similar to the neurons of the CNS, the differentiating factors between their milieus result in EN behaving very differently when cultured *in-vitro*, a factor which has limited research in field of gastroenterology.

1.5 Role in Disease States

The ENS has been shown to play a critical role in many diseases of both the gastrointestinal tract and the central nervous system. Since the ENS and the CNS have many signaling pathways in common, a lot of primary disorders of the central nervous system have enteric manifestations [20]. However, in many cases the exact role of the ENS and how it factors into the symptoms of different pathologies remains unknown.

For example, Hirschprung's disease is a congenital disorder characterized by the absence of EN in the distal colon, resulting in life-long abnormalities and a risk of incontinence. The lack of neurons prohibits signal transmission through the colon and impedes muscle contraction required for bowel movements. Similarly, enteric neurons in individuals suffering from Crohn's

disease and Irritable Bowel Syndrome have been shown to have decreased motility. This type of issue has also been shown to be a factor in Parkinson's and Alzheimer's diseases, neurological disorders, but the exact causal link has yet to be established [20].

The aforementioned diseases represent only a sub-set of those which are affected by alterations in the ENS, and do not currently have successful long-term interventions to eliminate and appease gastro-intestinal symptoms. This highlights the need to expand the current understanding of the ENS and how it factors into disease states.

1.6 Enteric Nervous System: Physiology and State-of-the-art

Neurons communicate through the transmission of electrical signals as a result of the movement of ions across their plasma membranes [21]. The presence of external stimuli initiates a cellular response that results in membrane depolarization, effectively initiating a physical response [22]. This change in the polarity of the membrane is referred to as the action potential and is the basis of neuronal activity, as well as the study of neurons [23].

In neurons, the action potential serves to propagate signals between each other by sending them down their axons to the axon terminals. The action potential is defined by the fluctuation of voltage across the membranes of neurons and the mechanism is the same in the ENS as in other nervous systems within the body, as shown in Figure 1 [7].

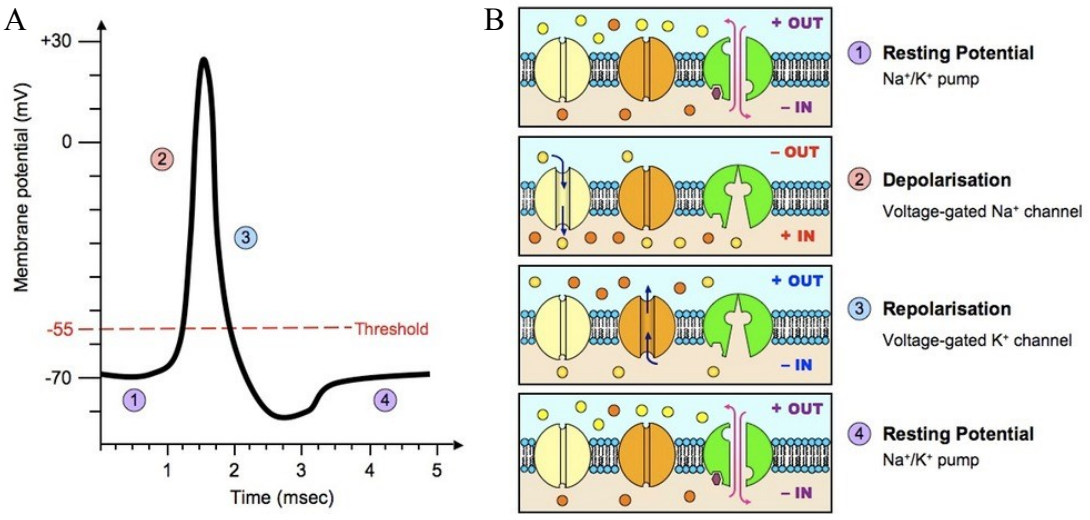

Figure 1. An overview of the action potential as a function of the variation of membrane potential with time (A). This rapid increase and subsequent decrease in potential is referred to as a 'spike' and the rate at which they appear is the 'firing rate'. The depolarization and polarization events correspond to the opening and closing of sodium gated channels as denoted in B. Image source: [24].

The electric potential of the plasma membrane is determined by the flow of ions across various voltage-gated channels. At rest, sodium voltage-gated channels are closed and the membrane potential is negative because of the primary movement of potassium ions from the cell into the cytosol. If a change is detected in the environment, sodium channels on the membrane will open while the potassium channels close, resulting in the increased flow of Na^+ ions out of the cell and a slight depolarization of the membrane. If this initial depolarization reaches a minimum threshold, it will further trigger the opening of more sodium voltage-gated channels, resulting in a large influx of sodium ions and a substantial depolarization surrounding the plasma membrane. The depolarization will also open the voltage-gated potassium channels causing potassium ions to flow and re-induce a hyperpolarization of the cell, while the sodium channels close. This results in the return to the resting state and the end of the action potential event [21, 23]. Action potentials are 'all-or-nothing' responses such that their power is not

proportional to that of the stimulus, but will not occur if the stimulus does not meet the minimal threshold value.

The shape, rate, firing pattern, and magnitude of action potentials are not uniform, but rather vary based on the type of neuron, the neurotransmitters at play, as well as the role of disease [25]. It has been shown that action potential firing rates are altered in many neurological disorders including epilepsy, Parkinson's, and in cardiac diseases due to changes in ion channels [26, 27]. Accordingly, there are many tools in place to be able to study the electrophysiology of neurons to gain insight on how their intracellular processes and neuronal networks manifest into physiological functions. Although it is known that dysfunction within the ENS is linked to gastro-intestinal disorders, our understanding of the electrophysiology behind the connection is limited [28].

The electrophysiology of neurons can be measured either using optical imaging, intracellular recordings, or extracellular recordings [29]. Optical imaging is performed using a fluorescent marker to tag intracellular calcium in order to visualize the movement of the calcium ions. Calcium plays a major role in signaling between neurons, and as such, the tracking of its spatiotemporal characteristics is utilized to correlate neuronal firing with biological models for disease and pharmacological studies [30]. However, the movement of calcium signals when triggered by action potentials is generally slow, limiting the reliability of reconstructing firing patterns [31]. Intracellular recordings often isolate single neurons and apply a sharp electrode to measure the current passing through a single cell. Although the readings are very accurate, this method limits the number of neurons that can be used to record data at once [29, 32]. This limitation is overcome with the use of extracellular recorders, such as multichannel microelectrode arrays (MEAs), which are able to record activity from networks of neurons

simultaneously. The use of extracellular readers also allows for the measurement of activity over longer periods of time without damaging the plasma membrane of the neurons [29, 31].

MEAs most commonly consist of glass wells with electrodes embedded within them, as shown in Figure 2**.** The electrodes are capable of providing electrical stimulation to the neuronal networks and recording the neuronal activity [33, 34].

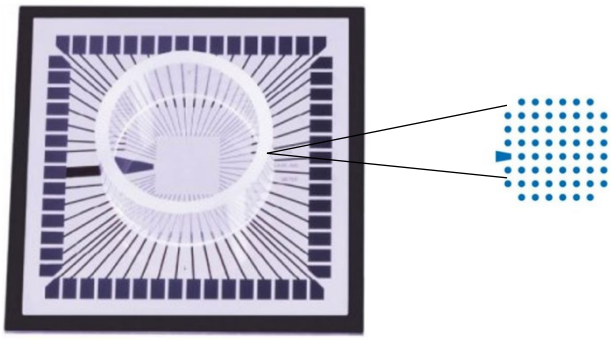

Figure 2. A standard single well MEA with a square recording area embedded with 64 electrodes in an 8x8 grid (insert) [35].

MEAs are generally coated with a protein layer in order to increase the adhesion of the neurons to the surface and promote the stability of the culture [32]. The coatings are often extracellular matrix type proteins and cell culture adhesion factors, but the use of carbon nanotubes has also been reported [29]. While this methodology is generally straightforward, it poses significant challenges when using enteric neurons, as they do not as readily adhere to the MEA's glass surfaces. In addition, common substrates used successfully on plastic tissue-cultureware do not perform as well in promoting the adhesion of the enteric neurons on glass, thus very few studies have been reported to be able to study ENS electrophysiology.

1.7 Neuron-Substrate Interactions

Neuron interactions with tissue within the body are largely mediated by the extracellular matrix (ECM) which consists of mixtures of proteins and complex saccharides that occupy

interstitial space. The components of the ECM are the result of secretion from cells, and aid to regulate neuronal maturation and the extension of axons [15]. In particular, certain ECM proteins components such as laminin and collagen, as well as proteoglycans (proteins bound to polysaccharides) have been shown to be effective in promoting neuron adhesion *in-vitro*. These same studies have also demonstrated that the neurons do not mature when cultured without the use of an adhesive substrate [15, 36].

In addition to substrate composition, it has been shown that cells respond to changes in stiffness, nanoscale features in the topography of surfaces, and chemical signals. Surface topography influences cellular processes such as differentiation and migration; however, very little is known about the effect of these factors on enteric neurons [15, 16, 37–39]. Both topography and stiffness can be measured by using atomic force microscopy (AFM), an imaging technique that can acquire three-dimensional images of surface topographies with nanometer resolution. AFM employs a cantilever with a small tip (Figure 3) which has a laser positioned onto it. As the tip moves across a surface, it forms weak interactions with the topographical features and causes the cantilever to bend in response, also resulting in deflection of the laser light [40, 41]. The deflection can be used to calculate stiffness, further discussed in Chapter 3.

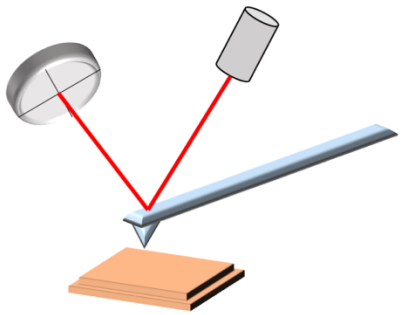

Figure 3. Schematic of AFM set-up with a sharp tip attached to a long cantilever which comes into contact with a substrate. A laser is positioned onto the cantilever at the location of the tip and deflects towards a detector which records the changes as a function of the interaction force between the tip and the surface.

Similar to stiffness, the topography of a surface can be tailored to design a particular pattern or to tune the dimensions of selected surface features. One means of doing so is with the use of polymer blends, consisting of polymers that are immiscible with one another and that separate into phases. When spin-coated, the polymers form a non-equilibrium film as the volatile solvent evaporates quickly, immobilizing the polymers onto the surface before equilibrium can be reached and resulting in the formation of unique morphologies [42, 43].

The degree of segregation in the blends plays a role in determining the morphology of the thin films, which also depends on a number of experimental factors including the polymers used, the composition of the blend, and whether the samples are annealed [44]. The ability to tune these surface structures has resulted in an increasing interest in the applications of thin films in the design of photovoltaic devices, semiconductors, and light emitting diodes [45]. However, they also serve as a platform to create surfaces that mimic intestinal environments in order to evaluate the effect of surface morphologies on the response of enteric neurons.

While a variety of polymers can be applied, two of the most common multipurpose materials are poly(styrene) (PS) and poly(methyl methacrylate) (PMMA)) [46]. However, while these polymers are biocompatible for certain cell lines, they have also been reported to interfere with cell viability. Accordingly, for their application in the study of enteric neurons, the surface of the polymer thin films should be functionalized with a material that is known to provide beneficial surface chemistry [47, 48].

The response of neurons to changes in their environment is critical for both physiological and pathological processes. The cells detect chemical signals, differentiate them, and relay the relevant information to the rest of the nervous system, initiating a migratory response or chemotaxis [49]. Neuronal migration as a result of chemical signaling is essential in the

formation and functioning of the nervous system and is a primary determinant in various human disorders. Disruptions in migrational processes resulting in flawed neuronal positioning is a cause of diseases such as autism and epilepsy, while an increase in migration towards damaged areas is important in cancer metastasis and tumor growth [50–52].

A variety of methods have been developed to study chemotaxis, and of interest is the use of biochemical gradients which mimic chemotaxis in the body and act as models to study neuron maturation and cell migration responses [51]. Studies of the central nervous system have shown that neurons cultured on glass fibres coated with ECM proteins such as laminin or fibronectin demonstrate migration, suggesting that these are effective substrates for studying neuronal chemotaxis [53]. However, the knowledge of the mechanisms controlling migration is limited, especially in the context of the enteric nervous system. Accordingly, these ECM proteins can be immobilized on a solid substrate as a means of investigating the response of enteric neurons to surface chemistry in order to elucidate a relationship between *in-vitro* migration and responses to chemical signaling in the body. Gradients can be created with the use of microfluidic devices where the intrinsic length scale is varied while other properties are maintained [54].

While it is known that the ENS plays a role in many diseases both of the central and the peripheral nervous systems, the direct cause of many pathologies remains unknown, mostly due to the limited understanding of enteric neurons. Accordingly, this has limited the development of effective treatments such that most disease interventions are therapeutic rather than curative. This work aims to apply a variety of experimental methods to probe the response of neurons to various substrates to understand how enteric neurons behave on a more fundamental level. The intent is to combine the findings with other work being performed by CHEO to standardize treatment of gastro-intestinal disease and develop tissue engineering based approaches.

Chapter 2- Materials and Methods

2.1 Material and Substrate Preparation

Chitosan-coated substrates

A 0.2% w/v solution of dopamine (Sigma-Aldrich) was prepared in 10 mM Tris buffer (Sigma-Aldrich) with pH 8.5 to enable the adhesion of chitosan to standard glass substrates. To this end, glass coverslips (12 mm, VWR) were immersed in the solution and covered overnight, followed by rinsing three times with deionized water. A 2% w/v solution of medium molecular weight chitosan (Sigma-Aldrich) was prepared in 1% acetic acid and stirred overnight then subsequently filtered through filter paper. Successively, either 0.5% wt genipin (Sigma-Aldrich) or 2% wt genipin, a naturally occurring cross-linker for chitosan-based hydrogels [55], was added to the chitosan solution under continuous stirring at room temperature for 3 or 6 hours. 150 μL of the resulting solution was pipetted onto the dopamine coated slides and the slides were left to dry at room temperature overnight.

Collagen-coated substrates

Glass coverslips were coated with polydopamine and with 150 μL of 100 μg mL^{-1} collagen type IV (Enzo) at room temperature, overnight, then rinsed with PBS.

Laminin-coated substrates

Glass coverslips were coated with polydopamine and with 150 μL of poly-D-lysine (Sigma-Aldrich) diluted to 0.1 mg mL^{-1} at room temperature, overnight. Subsequently, the poly-D-lysine was washed with PBS and the coverslips were coated with 150 μL of 0.1 mg mL^{-1} laminin (Sigma-Aldrich) at room temperature for 2 hours, then rinsed with PBS.

Matrigel-coated substrates

Matrigel® (Corning Life Sciences) samples were prepared over ice by mixing 30 μL in 170 μL of culture media and coating the solution onto glass coverslips that had been pre-coated with polydopamine. The coverslips were incubated at 37°C for three hours prior to culturing.

Block polymer Blend Sample Preparation

1% w/v solutions of polystyrene - PS (MW 35, 192, 280, 350 kDa; Sigma-Aldrich) and polymethylmethacrylate - PMMA (MW 120 kDa; Sigma-Aldrich) were prepared in toluene, and combined at various ratios. 60 μL of the solutions were spin-coated (Laurell WS 650) at 3000 rpm for 60 seconds on No.2 glass coverslips (VWR) and annealed (Shel Lab) at 160°C for 1 hour. The effect of a random brush layer was evaluated by spin-coating a 1% solution of a PS-r-PMMA (59 mol% PS; Polymer Source Inc.) at 3000 rpm for 60 seconds on the glass coverslips and annealing at 150°C for 1 hour prior to the coating of the blend.

Atomic Force Microscopy (AFM)

A WITec Alpha 300 integrated microscope (Witec, Germany) was used in Digital Pulsed Force Mode (DPFM) to collect images of the prepared coatings using a cantilever with a tetrahedral tip with a nominal spring constant of 2.8 N m^{-1} (Nanoworld, Switzerland) at a frequency of 900 Hz. This setting was applied for work on both **Objectives 1** and **2.** Force-displacement curves (Figure 4) were obtained from the DPFM data to determine the Young's modulus, which relates the tensile stress of a material to strain by fitting to the spherical Hertz model, equation 1, according to a procedure described by Fortier *et al.* and using OriginPro software [55]. The stiffness value was obtained by calculating the slope of the indentation portion of the curve.

$$F = \frac{E \tan \alpha \, \delta^2}{\sqrt{2}(1-\nu^2)} \quad [1]$$

where F is the force applied, E is the Young's modulus, ∝ is the face angle of the cantilever, δ is the indentation depth, and v is Poisson's ratio. An average of 10-15 curves were collected for three coverslips for each sample.

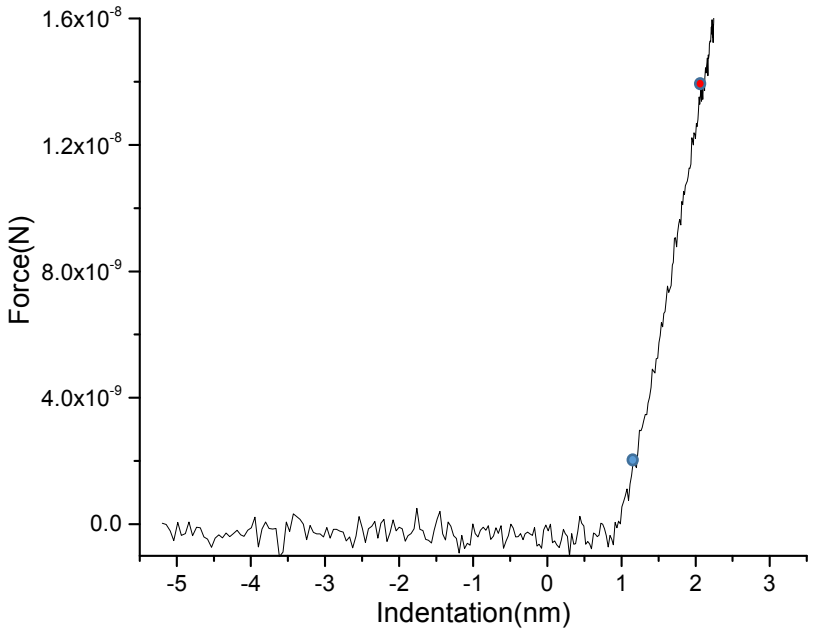

Figure 4. A force indentation curve with two points selected for fitting analysis; one at approximately 10% (blue) of the curve, with the other at 90% (red) of the curve.

Fourier Transform Infrared Spectroscopy (FTIR)

Sample stability and chemical composition for both **Objectives 1** and **2** were evaluated using a Bruker Tensor 37 FTIR spectrometer (Bruker USA) with a 2-mm diameter single reflection diamond crystal. A glass sample was used as a reference and readings were collected with 256 acquisitions per spectrum with a 4 cm^{-1} resolution. Data was acquired across 3 samples per condition and processed in OriginPro. The baseline was subtracted from the data, followed by smoothing with a Savitzky-Golay filter.

Gradient Substrate Preparation

Glass coverslips for **Objective 3** (75 x 25 mm, Corning) were sonicated for 5 minutes in ethanol, followed by 5 minutes in Milli-Q water (Millipore Corporation).

Mold Preparation

Molds were prepared by the Martinez Group at the Institute for Bioengineering of Catalonia (IBEC, Spain) by using the following protocol: A SU-8-2015 (Microchem Corp.) master was obtained using photolithography and then nano-embossed on a PEN sheet to obtain a negative replica by applying 70 bar of pressure at 200 °C for 30 minutes. The negative replica was subsequently used to transfer the structures to a PMMA substrate using nanoimprint lithography (Obducat AB, Sweden) by applying 30 bar of pressure at 125 °C. The microstructures on the replicas were characterized using AFM (Digital Instruments). The resulting molds contain Y-channels of 500 μm in width, 30 mm in length, and 70 μm in height.

Chip Preparation

PDMS prepolymer (Dow Corning) was mixed in a 10:1 ratio with a base polymer and degassed under vacuum for 1 hour. The prepolymer was then poured over the mold and cured at 65 °C overnight. Once cured, the chip was further prepared in a clean room by placing a cleaned glass slide overtop of the mold and cutting around its edges with an X-acto knife. The PDMS chip was then carefully removed with tweezers.

Glass top

A rectangular glass slide (VWR) was marked with 3 spots based on the template used in the mold. The slide was then placed in a plastic chamber with water, and the marked areas were drilled until a hole was formed.

Microfluidic Devices

Holes of 1 mm in diameter were punched into the chip (Ted Pella) to match those in the glass tops then tubing of inner diameter 0.5 mm and outer diameter 1 mm was pushed through them (Sigma-Aldrich). The chip was placed atop of the pre-drilled glass slide and the tubes were fed through the holes in the glass. The ends of the tubes were trimmed to a workable size and 23G 1" needles (BD Microlance) were fed into the ends.

Protein Gradients

A prewashed glass slide was placed atop of the PDMS chip and the two were sealed with four binder clips, arranged such that they did not block the channels. The two entry needles were attached to 5 mL syringes (12.5 mm, BD Discardit), one of which was filled with PBS and the other with the required volume of laminin protein. The syringes were both positioned into respective microfluidic pumps, while the third exit needle was placed into a glass bottle to collect the exiting waste. The fluidic system was left to run to check for leaks and the flow rates of the pumps were varied to develop a linear gradient, as per the times shown in Table 1. The parameters were optimized by the Martinez Group at the Institute of Bioengineering of Catalonia in Barcelona, Spain. Once complete, the slide was carefully removed from the PDMS chip and washed, protein side facing up, with both PBS and MilliQ, The gradient was visualized with fluorescence imaging and the analysis was performed in ImageJ®.

Table 1. Time and flow rates for both the protein and PBS filled syringes to be pumped to form a linear protein gradient.

Time (min:sec)	Protein (uL/min)	PBS (uL/min)
0	10	90
7:56	20	80
14:56	30	70
21:06	40	60
26:15	50	50
30:41	60	40
34:01	70	30
36:35	80	20
39:01	STOP	50
44:01	STOP	STOP

2.2 Enteric Neuron Cultures and Cell Studies

Isolation

Enteric neurons were isolated and cultured according to the protocol developed by Wahba *et al* [11]. Adult CD-1 mice (Charles River) were euthanized by cervical dislocation and the small intestine was removed and placed in Krebs-Ringer solution (126 mM NaCl, 5 mM KCl, 1.2 5mM Na_2HPO_4, 1.25 mM $MgCl_2$, 2.5 mM $CaCl_2$, 11 mM glucose, 25 mM $NaHCO_3$). The intestine was washed with the Krebs-Ringer solution using a 20-gauge feeding needle (Fine Science Tools) and cut into 4 pieces. The segments were then placed in a 10-cm dish with a silica base (Dow Corning) containing Krebs-Ringer solution. The longitudinal muscle and myenteric plexus (LMMP) were separated from the remaining gut layers using gentle abrasion with a pair of curved forceps (Excelta 7-SA) and stored on ice in a 15 mL conical tube containing Krebs-Ringer solution until further processed.

Culture

The 15-mL conical tube was centrifuged at 200 g for 5 minutes, and the supernatant was aspirated. The pellet was suspended in collagenase (2 mL of solution per mouse; 1 mg/mL collagenase IV, 0.5 mM $CaCl_2$, 10 mM HEPES in HBSS) and incubated in a 37 °C water bath for 15 minutes while stirring. The tube was then centrifuged at 200 g for 5 minutes and the supernatant was aspirated. The remaining tissue was washed in filtered HBSS for 5 minutes with shaking, and the pellet was left to settle. The supernatant was aspirated and the step was repeated. The pellet was suspended with trypsin solution (1 mL of solution per mouse; 0.05 % Trypsin, 0.53 mM EDTA in HBSS) and incubated in a 37 °C water bath for 10 minutes while stirring. The tube was then centrifuged at 200 g for 5 minutes and the supernatant was aspirated. The resulting pellet was then triturated in culture media (2% v/v fetal bovine serum, 100

units/mL penicillin, 100 µg/mL streptomycin, 1X B27 supplement, 1X N2 supplement, 7.2 mg/L uridine triphosphate, 15.6 mg/L 5-flurodeoxyuridine, 2.5 mg/L amphocetrin, 50 mg/L gentamycin sulfate in DMEM/F12 media) with a 1 mL pipette and diluted for plating.

Immunofluorescence Imaging

The cells were cultured on the substrate coatings in 24 well dishes (VWR) between 1 to 3 weeks with daily media changes. Cells were fixed in 4% paraformaldehyde with 7% v/v picric acid for 20 minutes at room temperature and then incubated overnight with primary antibody staining for neuron specific beta-tubulin, Tuj-1 (gift from Dr. A. Frankfurter) at 4°C. The cells were then rinsed with PBS and incubated with secondary antibodies (Life Technologies) for 30 minutes at 37°C. All of the antibodies were diluted in PBS with 0.3% Triton-X. The glass slides were mounted onto coverslips (VWR) and imaged on a Zeiss AxioObserver.Z1. The images obtained were analyzed using ImageJ to determine the percentage surface area covered by neurons and neurites, respectively.

Live Imaging

The cells were seeded onto the substrate in a 2-well chamber slide (ThermoFisher) and left overnight to allow for a media change. A phase-contrast image was taken every 30 minutes over the course of 72h with a Zeiss AxioObserver-Z1. Humidity and carbon dioxide levels were controlled with the use of a humidified incubation chamber, while temperature was maintained at 37 °C with a heating unit.

Scanning Electron Microscopy (SEM)

Fixed samples were dehydrated by immersing them in increasing concentrations of ethanol ranging from 30% to 100% over 30 minutes then gold-sputtered to minimize charging

effects from organic protein. Imaging was performed by the Materials Characterization Facilities on a JSM-7500F Field Emission Scanning Electron Microscope (FE-SEM).

Multichannel Microelectrode Arrays (MEAs)

Prior to use for **Objective 1**, the MEAs (MultiChannel Systems) were washed with Terg-A-Zyme (Sigma-Aldrich) while shaking, then subsequently rinsed with de-ionized water and allowed to soak in ethanol overnight. The cells were plated onto coated MEAs consisting of 60 titanium nitride microelectrodes, 30 μm in diameter and 200 μm apart. Potentials were recorded with a sampling frequency of 50 kHz, and stored using the MC_Rack software provided by MultiChannel Systems. The spiking data obtained was analyzed using SpAnNer (Result Medical, Germany). The cells were treated with 3, 10, and 30 uM of nicotine in order to up-regulate their activity (gift from Dr. William Staines) based on methodology described by Galligan [56].

Statistics

All experiments were performed in triplicate with three samples per condition. Data were plotted on a histogram to confirm whether it was normally distributed. Normalization was further evaluated using the skewness and kurtosis values. A one-way ANOVA and a post-hoc Tukey test was applied to determine the presence of statistical significance between the data points.

Chapter 3- Objective 1: Results and Discussion

3.1 Substrate evaluation

Current methodologies for the culturing of enteric neurons rely on the use of plastic tissue cultureware and do not report success on the use of glass [6, 11]. However, the use of MEAs to study the electrophysiology of the neurons and their response to environmental changes requires the cells adhere to glass with embedded electrodes. Initial attempts were made to utilize the same adhesion materials used in standard cell culture, namely laminin, poly-D-lysine, matrigel, and collagen, on glass but these were unsuccessful in adhering the cells to the glass for more than 3 days. This indicated that there were factors either in the material properties of the underlying substrates or in the interactions of the adhesion factors with the substrates that impeded the enteric neurons from binding.

As such, a variety of biomolecules were selected for their evaluation in the use as an adhesive material for the enteric neurons on glass. A summary of the materials used and their general applications is shown in Table 2. The materials selected either have known use in current biomedical applications, such as chitosan and polydopamine, or are popular tissue culture materials.

Table 2. Summary of materials applied to glass substrates to promote adhesion of enteric neurons during cell culture

Material	General application
Chitosan	Aminopolysaccharide derived from crustacean shells gaining popularity as a biomaterial [57]
Genipin	Plant extract with use as a non-toxic crosslinking agent [58]
Polydopamine	Bio-inspired polymer with strong adhesion properties [59]
Matrigel ®	A mixture of extracellular matrix proteins rich in laminin and collagen (Corning® Product)
Laminin	Extracellular matrix protein commonly used in tissue culture
Poly-D-lysine	Amino acid used as an attachment factor in conjunction with laminin
Collagen	Extracellular matrix protein commonly used in tissue culture

Each of the materials was prepared as described in Chapter 2 and their topography was profiled with AFM. The materials were either coated onto the glass directly, or onto glass that had been functionalized with polydopamine. Under alkaline conditions, dopamine undergoes a polymerization resulting in polydopamine, which has been shown to promote *in-vitro* cell development. It demonstrates adhesion properties on both hydrophilic and hydrophobic surfaces and is effective in functionalizing surfaces for cell studies [60]. Through AFM, the topography of the surfaces was visually compared to that of glass to gain an understanding of the general surface features and their size, shown in Figure 5.

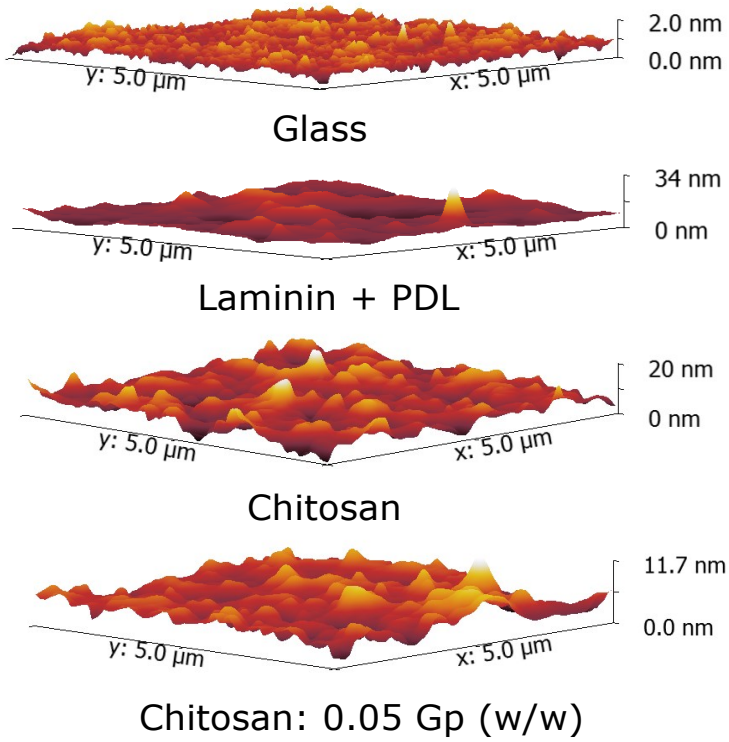

Figure 5. Topography maps obtained with digital pulsed forced mode AFM for glass, glass coated with laminin and poly-d-lysine, chitosan, and chitosan cross-linked with 0.05 wt% genipin.

All of the protein coatings described in Table 2 demonstrated similar topographies with AFM, thus only that of laminin is shown above. Laminin has a uniform surface and appears to take a relatively flat morphology at the nanoscale while the chitosan surface was more granular.

Coating the glass substrate increased the height of its surface features, from an upper limit of 2.0 nm on glass, to 34 nm on glass with laminin and PDL. The protein-based surfaces also had surface features that largely exceeded those of the chitosan by upwards of approximately 14 nm.

Cross-linking chitosan with genipin, a naturally occurring cross-linking molecule for chitosan, was found to decrease the height of its surface features and resulted in a slightly less granular appearance, indicating that the addition of genipin results in more compact packing of polymeric chains [61]. In fact, introducing genipin into chitosan mixtures results in a cross-linking process depicted in Figure 6 where the chitosan chains are joined together [58]. This process introduces covalent bonding while maintaining the non-toxicity of the substrate, and in turn increases the stiffness of the chitosan. The degree of increase in the stiffness value varies depending on the amount of genipin added and the length of time it is stirred into the chitosan [62, 63]. Accordingly, this method was used to evaluate how material stiffness affects enteric neuronal cell differentiation.

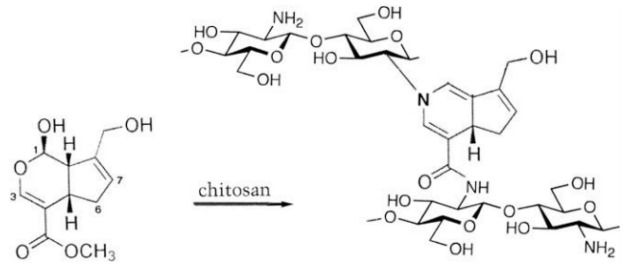

Figure 6. One mole of genipin cross-linking two chitosan chains [58]

AFM was used to collect force versus extension curves which were fitted to the Hertz model to determine the Young's modulus (E) and stiffness of normal and cross-linked chitosan, Figure 7.

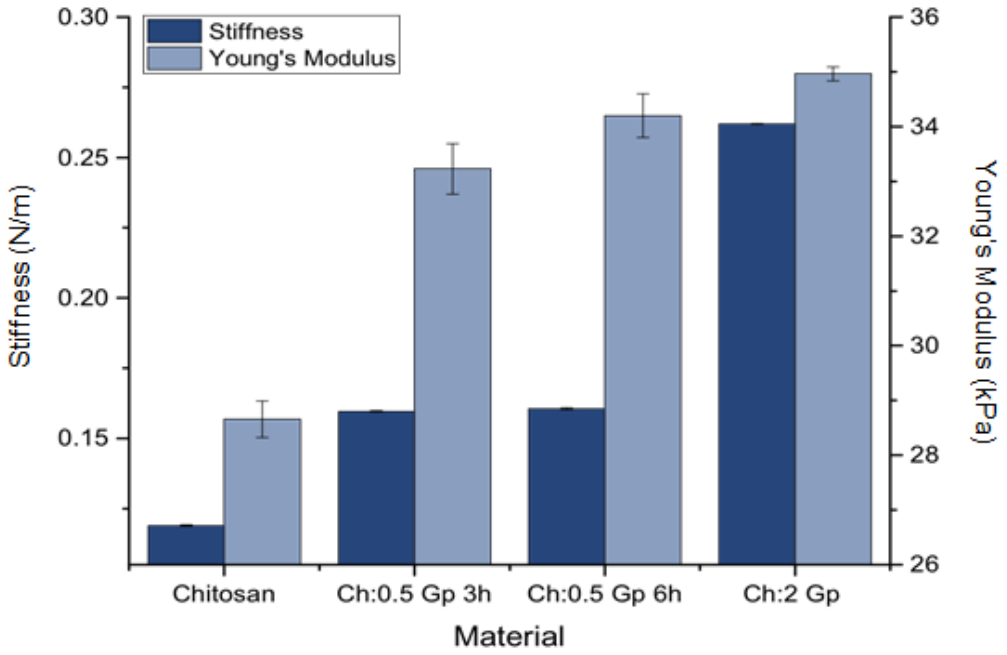

Figure 7. The effect of stiffness on neuron binding was assessed by cross-linking chitosan (Ch) with varying concentrations of genipin (Gp), stirred for either 3 or 6 hours. Concentration designations (0.5 or 2) are a weight percentage of genipin relative to chitosan and error bars denote standard deviation.

One-way ANOVA tests ensured that differences between the samples were statistically significant ($p < 0.05$) between all conditions relative to chitosan for both the stiffness and the Young's modulus E. However, in the case of E, none of the cross-linked conditions were statistically significant relative to each other, as was in the case of stiffness for the two 0.5 wt% conditions. The untreated chitosan sample had the lowest average stiffness and E values of 0.119 N/m and 28.6 kPa, respectively. By increasing the degree of cross-linking, the average stiffness and E values of the substrates increased up to 0.262 N/m and 35 kPa, respectively, for the two percent genipin condition. This finding was expected as the introduction of genipin results in the formation of covalent bonds within the sample, which strengthens the interactions between the chitosan molecules. In addition, the E values determined fall within the order of 10 kPa, which is the same order of magnitude as other reports which have evaluated chitosan under similar conditions and using AFM [62, 64, 65].

However, it is noteworthy that others have reported Young's modulus values for chitosan in the range of MPa [66]. The magnitude of difference in these calculated values and those reported by other groups may be due to limitations associated with fitting to the Hertz model, namely in the determination of a contact point. As the Hertz model is dependent on this initial estimation, the selection of the contact point can result in variance in the results. To maintain consistency, points in these calculations were selected at 10 percent and 90 percent of the force versus extension curves when calculating the contact point [67].

When the enteric neurons were cultured onto the materials of varying stiffness, the cells adhered onto chitosan but did not bind to any of the cross-linked conditions. This demonstrated that the enteric neurons preferred softer and thicker substrates which is contradictory with the preferences of other cell types and neurites that have been reported [68, 69]. This may be attributed to toxicity arising from the use of genipin, or substrate stiffness which exceeds that which the cells would normally be exposed to. Accordingly, the binding of the cells to normal chitosan was further used as a comparative condition.

The objective in culturing the enteric neurons on glass is to obtain adhesion and outgrowth properties that closely mimic those seen on plastic substrates as in Figure 8.

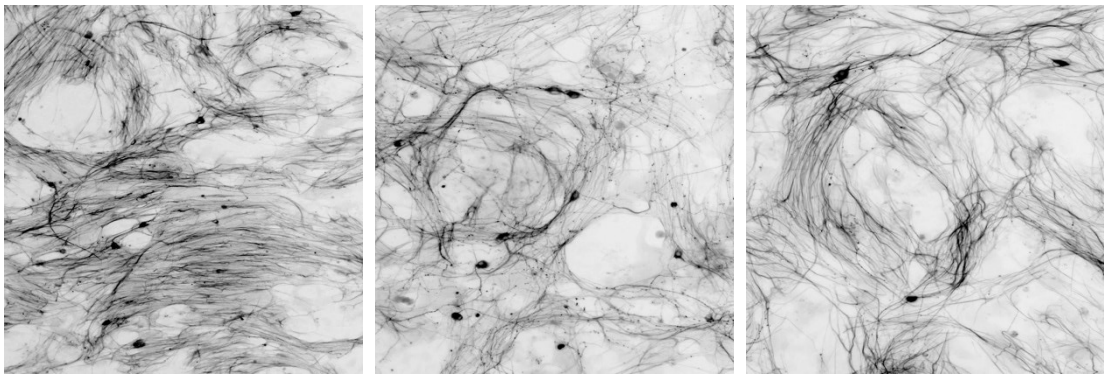

Figure 8. Enteric neurons at 10X magnification cultured using the described protocol on laminin and PDL coated plastic tissue cultureware substrates (Image courtesy of Children's Hospital of Eastern Ontario [11]).

Of particular interest to determine whether a substrate is beneficial are (*i*) a high number of neurons, (*ii*) an extensive neurite network to facilitate communication between cells and (*iii*) long-term adhesion. The cells cultured on plastic were generally able to survive for the length of their average lifetime of 3-5 weeks. Accordingly, the materials used on glass were evaluated based on their ability to support the aforementioned criteria. Figure 9 shows the immunofluorescence images of the binding of the enteric neurons to the most effective materials coated onto glass substrates.

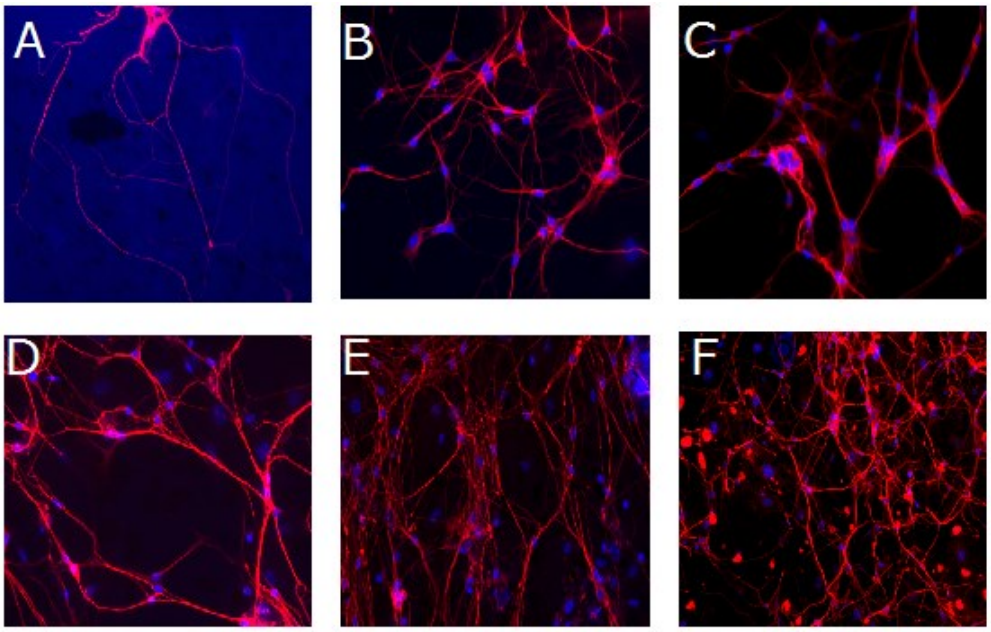

Figure 9. Immunofluorescence binding of the neurons on substrates: A. Chitosan, B. 75:25 Chitosan:Collagen, C. Collagen, D. Matrigel, E. Matrigel on polydopamine F. Laminin and PDL on PDA.

The different substrates tested were compared by quantifying, via image analysis, the percentage surface area covered by neurons and neurites, as shown in Figure 10. A one-way ANOVA test was carried out to assess the statistical significance of the results ($p < 0.05$). Results are summarized in the Appendix. Specific conditions, rationally selected to display the most significant variations recorded, have been highlighted in Figure 10, showing that neurons behaved differently in terms of forming complex networks in relation to the underlying substrate.

Of note, the use of PDA-immobilized matrigel resulted in the closer resemblance to binding on plastic (Figure 8).

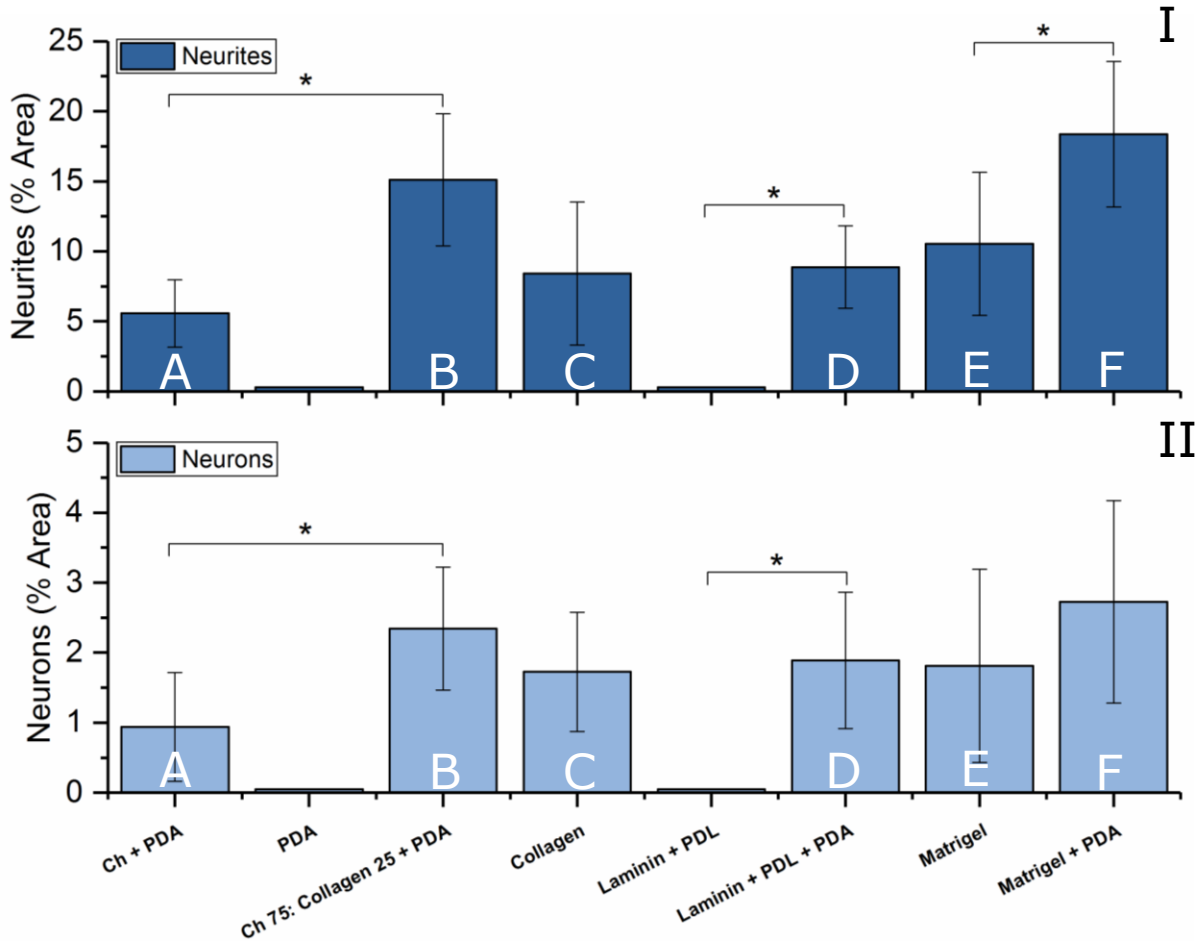

Figure 10. Number of neurites (I) and neurons (II) bound to the materials coated onto glass substrates calculated as a percentage of the surface area of the images analyzed. Ten images collected across 3 samples were averaged using ImageJ software. Error bars denote standard deviation.

All of the conditions were able to support the neurons for a minimum of three weeks, with most surviving up to 4.5 weeks. Based on the neurons and neurite analysis, the most effective condition was found to be PDA-immobilized Matrigel®. This condition was thus selected for the electrophysiology studies. However, since the resulting polymeric layer is relatively thick, it prevented the firing activity of the neurons from being captured by the

underlying MEA electrodes. For this reason, another condition that would create a thinner coating while supporting the neurons was selected instead. Figure 10 shows that neurons adhere nearly as well to the chitosan and collagen mixture as they do to Matrigel®. In this context, it should be noted that chitosan can only be removed from surfaces using an acidic treatment; a process that would risk damage to the electrodes on the MEAs for subsequent uses. Accordingly, the alternative of PDA-bonded laminin and PDL was chosen for use on the MEAs to ensure satisfactory neuronal attachment and reusability of the equipment. While PDA adhesion to glass is generally considered to be permanent, in preliminary studies it was determined that it could be removed using a 10X dilution of bleach in conjunction with Terg-A-Zyme detergent.

Of note, enteric neurons did not adhere to the laminin and PDL when they were coated on glass without PDA (Figure 10). This suggests a synergistic effect stemming from the use of PDA with the coating on the glass substrate due to the introduction of ligands on the glass substrate to promote the binding of adhesion receptors on the laminin protein. In addition, it was observed that cells did not adhere onto PDA, which may be attributed to the presence of fetal bovine serum (FBS) in the media. FBS is a serum supplement commonly used in eukaryotic cell cultures which contains various proteins that have the potential to bind to the bare PDA and block its binding sites from being accessible by the neurons.

After having selected a combination of laminin and PDL as the most effective alternative to glass to support neuron viability, a stability study was carried out to assess whether this was the result of improved adhesion onto the substrate. In fact, it could be envisaged that the better results achieved on the PDA-immobilized coatings are subjected to a less pronounced dissolution of the coating as a consequence of the adhesive properties of PDA. To demonstrate this aspect, laminin and PDL were coated onto glass substrates with and without dopamine. The substrates

were then investigated by using infrared spectroscopy after immersion in aqueous media for 7 days in order to detect variations in the chemical composition of the coating that could result in its dissolution [70, 71]. The change in infrared spectrum over such period is shown in the figure below.

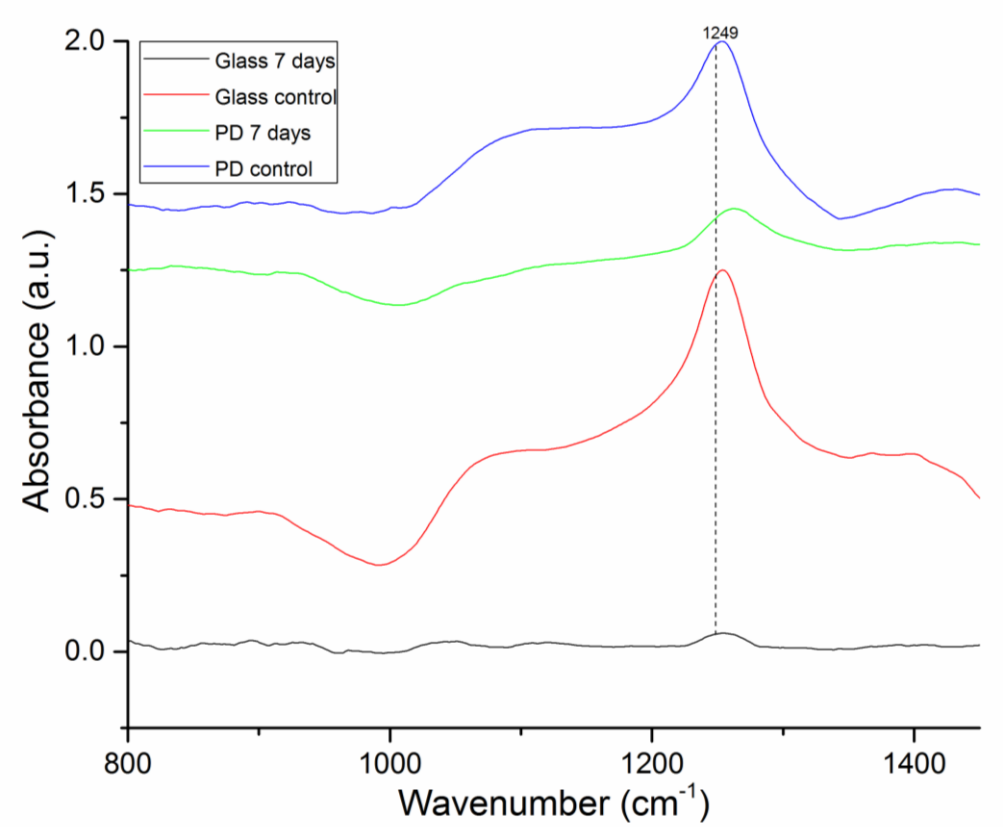

Figure 11. FTIR data to determine stability of laminin and PDL in aqueous media. The materials coated on glass with and without dopamine at t=0 are denoted in blue and red, respectively. At t=7 days, the condition without dopamine is shown in black, and that with is shown in green.

At t=0, the IR spectrum of glass both with and without dopamine appear nearly identical, with a prominent peak at 1249 cm^{-1}. This peak is due to the presence of a C-O-C bond which is present in PDL and its presence indicates that the laminin and PDL coatings are adhered to both substrates [72]. However, after 7 days, these features are undetectable in the glass-only condition. On the PDA-functionalized glass, the characteristic IR spectrum can be observed,

although its intensity is reduced, indicating that PDA helps retain the protein adlayer in an aqueous environment of culture medium. It is likely that the laminin and PDL are dissolved into the aqueous media and lost during replacement of the solution, or displaced by protein in the FBS within the media. Similarly, any cells bound to the polymeric coating would also be lost during the media change process, accounting for the lack of visible cells on the glass with laminin and PDL but without PDA.

Additional analysis of the neuronal binding onto the substrate was carried out to evaluate the degree of branching across the conditions in order compare the complexity of the networks formed. A more extensive network will result in more connection points among neurons and is expected to increase the amount of communication that can be captured by the MEAs during a reading. The branching complexity was determined using the NeuriteTracer® ImageJ plugin which traces all of the neurites and relates the number of branching points off each one to that neurite's length. Results are displayed in Figure 12, however, a one-way ANOVA test revealed that differences are statistically non-significant. This may be attributed to the degree of complexity in the images analyzed; the significant neurite overlapping makes it difficult to distinguish start and end points. As a result, in many cases the branching complexity may have been overestimated since certain neurite branches would be counted multiple times for the same intersection due to inherent limitations of the current ImageJ® plugin available.

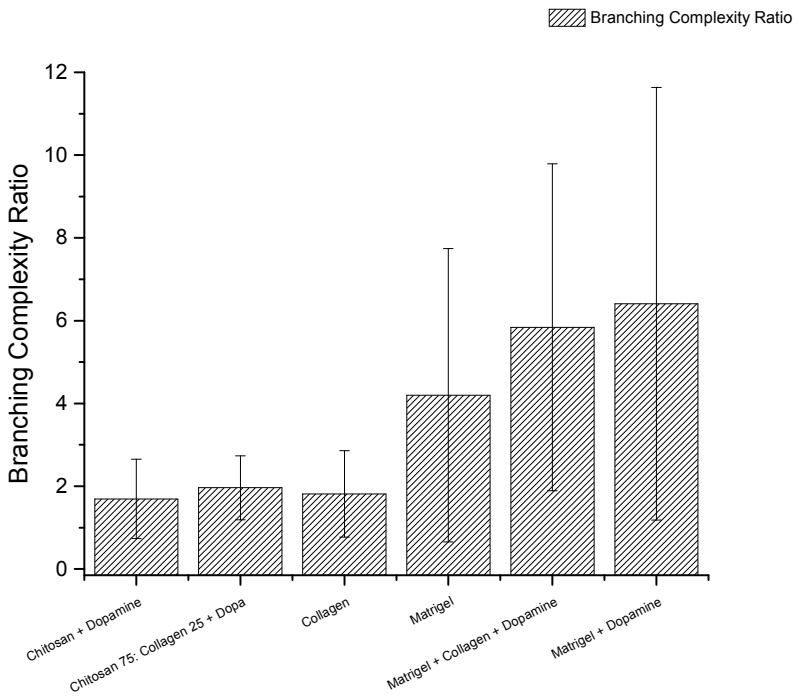

Figure 12. Branching complexity of the neurons and neurites determined using NeuriteTracer in ImageJ. This plugin traces the neurites and relates the number of branching points for each neurite relative to its length. The results are statistically non-significant ($p<0.05$) for all conditions with error bars denoting standard deviation.

An additional analysis was performed to relate the neurite outgrowth to the number of neurons as a means of standardizing the number of neurites per neuron. In this context, it could be conceived that while one substrate may not support neuron adhesion, it may nonetheless stimulate neurite outgrowth, and as such it would be useful to single out this factor during data analysis. Figure 13 shows the average value of neurites for each neuron on the different substrates. However, as in the case of branching complexity, all of the results were found to be statistically non-significant at $p<0.05$. Accordingly, only the percentage surface area of the neurons and neurites was utilized as an evaluative criterion in selecting the most suitable substrate for supporting enteric neuron adhesion and viability on MEAs.

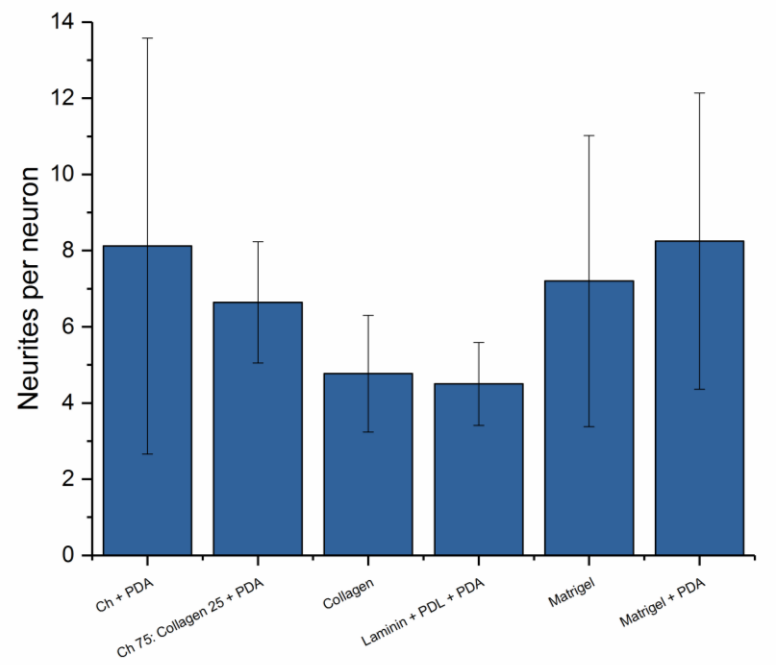

Figure 13. Average number of neurites per neuron for different substrates investigated. Results are statistically non-significant across all conditions as determined by one-way ANOVA test at $p<0.05$.

3.2 Electrophysiology of neurons on MEAs

The optimal substrate identified during the study of neuron binding described in Section 3.1 was successively used to coat the MEA's surface in order to enable electrophysiology studies. The MEA records firing activity that occurs at the location of the individual electrodes (black circles in Figure 14). Although the MEA contains 64 electrodes, it is imperative that the neurons adhere to them with a high density to ensure that their activity can be recorded.

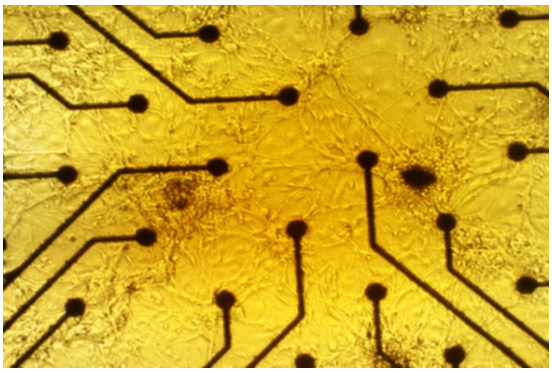

Figure 14. Optical image at 5X of enteric neurons adhering onto MEA glass surface coated with polydopamine, poly-D-lysine, and laminin. The black circles are electrodes, while the black lines are the electrical connectors that couple the electrodes with the plate readers.

The polydopamine, poly-d-lysine, and laminin coating was effective at both enabling neuron adhesion on the MEAs and supporting enteric neuron viability for approximately four weeks. Neurons were cultured and allowed to extend their neurites for 10 days in order to develop an elaborate network prior to any readings. After 10 days, MEAs could record electrical signals as shown in Figure 15.

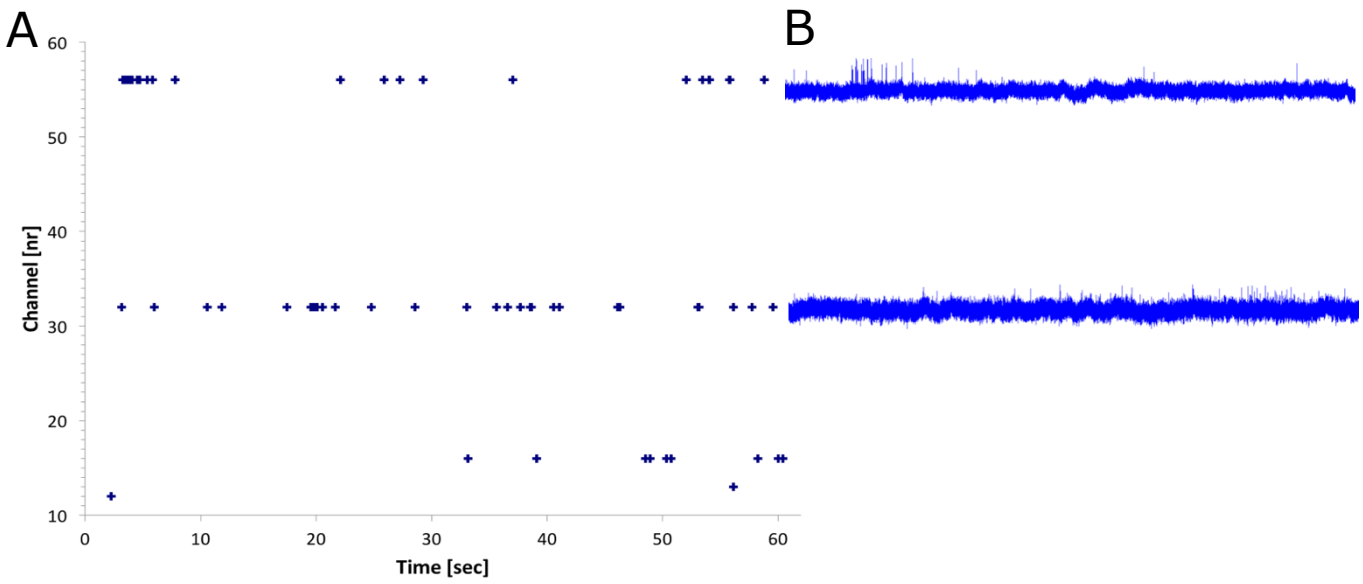

Figure 15. Neuronal activity was present on MEAs after 10 days when cultured on PDA-functionalized PDL and laminin. (A) Spiking rate was measured against time for firing across 3 electrodes. (B) Recording of activity at electrodes #32 and #52 over 30 s.

Figure 15A shows firing events over time for each of the MEAs electrodes, which are represented as channels on the y-axis. Each node on the graph denotes a change in voltage across the reader, indicating that a synapse has occurred. Figure 15B shows the readings for channels 32 and 52 over 30 seconds as it appears during the real-time recording; each spike is a change of voltage and the height of the spike is proportional to the degree of change. The average spike rate was 6.9 ± 18.5 spikes min^{-1} and 13.5 ± 23.9 spikes min^{-1} for channels 32 and 52, respectively. During trials and readings, the spike rates recorded varied but this is common across neurons. As neuronal activity is highly variable, the same neuron can produce very different spike patterns at varying rates under constant conditions. This variability can arise from a number of factors including fluctuations during the biochemical processes affecting firing [73]. It is generally not recommended to average spiking over multiple trials as it can mask temporal features. The spiking data presented above represents a single trial, but these results were consistent over multiple trials and over multiple days of reading. To mitigate excessive variation, the software

used to analyze the firing activity applied a smoothing function to eliminate noise from the data. While the aforementioned readings had markedly variable spiking rates, the values recorded fall within the range of those reported for cortical neurons of between 1-200 spikes/s [74, 75].

Similarly, the relative changes across voltage for each synapse is also variable between the spiking events, demonstrating that the activity of the neurons is not one-noted and that they are likely able to detect and react to physicochemical cues. Of note, this also indicates that the surface coating used on the MEAs does not impair the neurons' ability to communicate with each other.

The most firing recorded at once was for three electrodes (Figure 15). It is desirable to be able to increase the neuron density in order to read from more electrodes simultaneously, which may be accomplished by using a higher number of mice during the culturing process. A limitation of the culture method used in this work is that the cell number obtained through harvesting cannot be counted prior to seeding, such that it is not possible to control the number of cells being cultured onto a substrate. Similarly, proteins must reach receptors in specific conformation in order to be able to bind successfully; an aspect which cannot be predicted or controlled. Thus, one cannot know with certainty whether the amount of cells seeded will be sufficient for increased activity during electrophysiology studies. To overcome this issue, it will be necessary to refine the culturing method to account for differences across animal health, size and specific dissection protocols and techniques.

Based on the evidence that protein-functionalized MEAs can detect the electrical activity of neurons, nicotine was added into the culture media to determine whether our approach lends itself to *in-vitro* studies aimed at investigating the up-regulation of neuronal functions. Nicotine binds to and stimulates the nicotinic acetylcholine receptors (nAChR) in neurons, causing the

channels to open and to allow depolarization of the membrane. That depolarization, in turn, leads to the occurrence of action potentials and in the case of the myenteric plexus, longitudinal muscle contraction [56, 76]. The neuron firing rates were recorded pre and post treatment with 3 uM of nicotine (Figure 16).

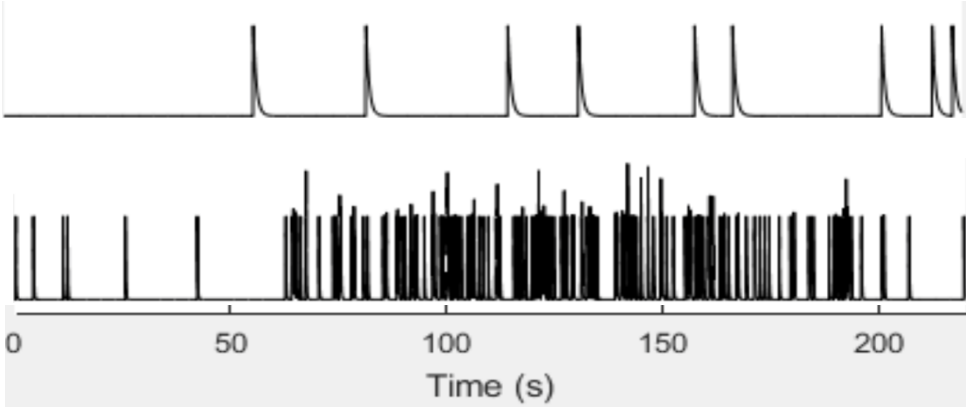

Figure 16. Enteric neuron activity recording in real-time over 200s. Top is activity of non-treated cells and bottom is activity following treatment with 3μM of nicotine.

Prior to treatment with 3 uM of nicotine, the neuron spiking rate was recorded at 0.045 spikes s^{-1} (Figure 16, top) and following exposure to nicotine, increased by 10 fold to 0.31 spikes s^{-1} (Figure 16, bottom). The neurons were further treated with 10 and 30 uM of nicotine, but this resulted in a suppression of activity. This was likely due to a shock response as these concentrations were not toxic and did not cause evident cell death.

The up-regulation shown above indicated that the surface coating used on the MEAs was effective at reading the true activity of the cells and could have further application in drug studies. This method allows for the assessment of the effectiveness of drug treatments in gastrointestinal disorders by studying them *in-vitro* using patient tissue samples or mutant animals. This permits better selection of the course of action when treating diseases with gut components without subjecting the patient to unwanted side effects associated with many pharmaceuticals.

Chapter 4- Objective 2: Results and Discussion

4.1 Polymer blend surfaces

The observations resulting from **Objective 1** indicated that the enteric neurons were sensitive to differences in the underlying substrate. For a better understanding of their functions, it was of interest to evaluate whether such differential response is related to topographical and/or chemical differences among the various substrates investigated. To this end, we isolated the effects of the topography by employing blends of poly(styrene) (PS) and poly(methyl methacrylate) (PMMA) which are immiscible and form unique surfaces of repeating patterns. These surface patterns can be fine-tuned and vary depending on the molecular weight (MW) of the polymers, the concentration, the annealing temperature and time, and the ratio of the polymers [42–44]. The resulting patterns were successively functionalized by laminin and PDA in order to maintain the surface chemistry consistent across different samples and thus single out the effects on the surface topography.

Initial studies were performed to evaluate how the composition of the blends affected the resulting surface topographies. Figure 17 shows the nanotopographies obtained by varying the ratio of PS to PMMA while maintaining other experimental conditions constant (i.e. concentration, molecular weight, annealing conditions).

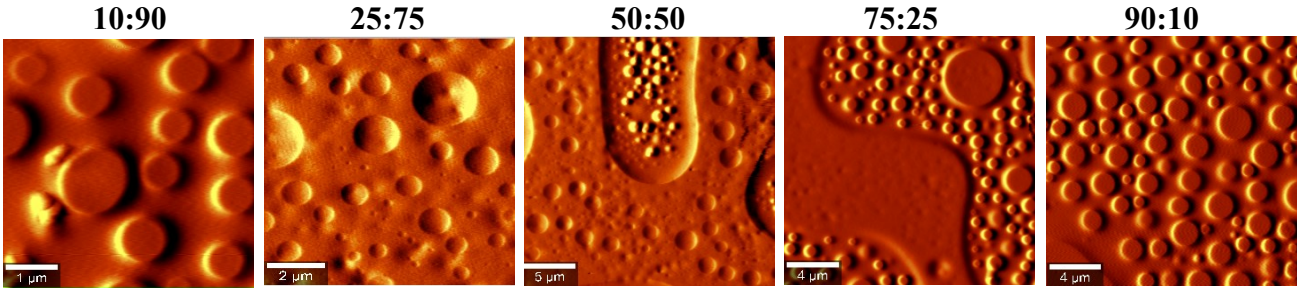

Figure 17. Effects of varying the ratio of PS:PMMA with PS with a a molecular weight (MW) of 192,000 and a concentration of 1% w/v. The samples were spin coated on glass slides and annealed at 160 °C for 30 minutes. The ratios are denoted on the image and varied from 10:90 to 90:10.

There was not an evident relationship between the structures formed as a function of the ratio. It was noted that the surfaces of 10:90 and 90:10 resembled one another with circular features, while the ratio of 75:25 showed the largest variability in dimension and structures. A similar comparison was carried out to investigate the effects of the concentration on the resulting surface nanotopographies (Figure 18).

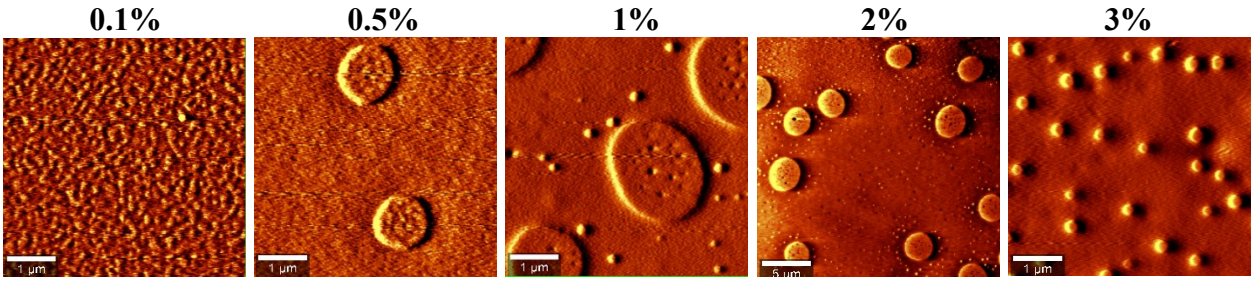

Figure 18. Effects of varying the ratio of PS:PMMA solution concentrations (% w/v) with PS with a MW of 192,000. The samples were spin coated on glass slides and annealed at 160 °C for 30 minutes. The concentrations are denoted on the image and varied from 0.1% - 3%.

Similar to the previous case, there was no clear trend to describe how surface features vary according to the concentration. At 0.1%, the surface displayed a granular morphology with no discernible patterns. As the concentration increased, circular protrusions with variable size and spatial arrangement formed, but no distinct patterns were observed [44]. Using the same

25:75 ratio and selecting a concentration of 1%, the influence of the MW was also investigated as a variable to fine tune the topography of the polymer blends (Figure 19).

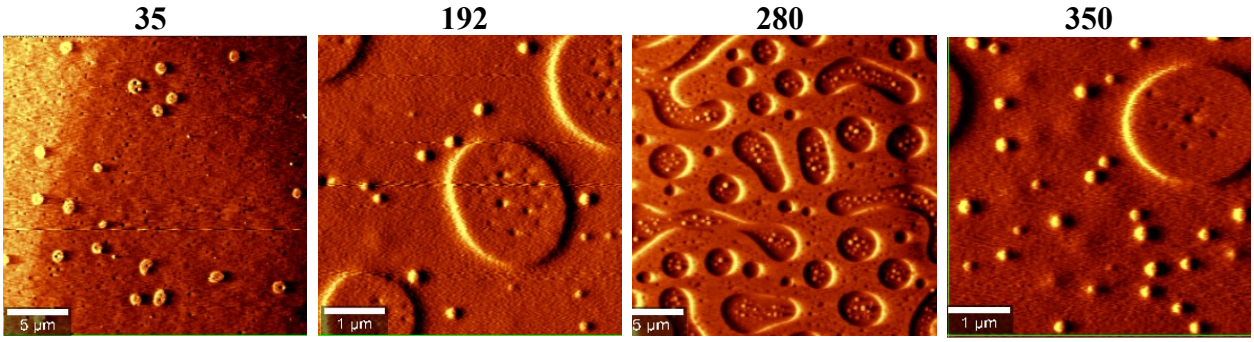

Figure 19. Effects of varying the MW of PS using a ratio of 25:75 and 1% w/v solutions. The samples were spin coated on glass slides and annealed at 160 °C for 30 minutes. The molecular weights are denoted (factor 1/1000) on the image and varied from 35-350.

At a low molecular weight (MW=35), the surface features were minimal across the surface and quite scarce, but these increased in size and frequency as the MW increased. Both MW=192 and MW=350 samples were indiscernible from one another, forming a combination of large and small protrusions, while at MW=280, the surface showed pitting. As in the previous cases, there was no clear link between the interplay between surface topography and concentration. In addition, all of the surfaces investigated (Figure 17-19) were annealed to bring them to a lower energy state. The annealing temperature can vary but it is usually above the glass transition temperature of the polymers, which are approximately 85 and 155 °C for PS and PMMA, respectively. The high temperature increases the diffusivity of the polymers and drives their segregation, which leads to self-assembly of the surface nano-patterns [77]. It also helps to bring them to equilibrium following solvent evaporation that occurs during the coating process [78]. Given the importance of the annealing temperature, we assessed its effects on the surface topography for a selected blend (Figure 20).

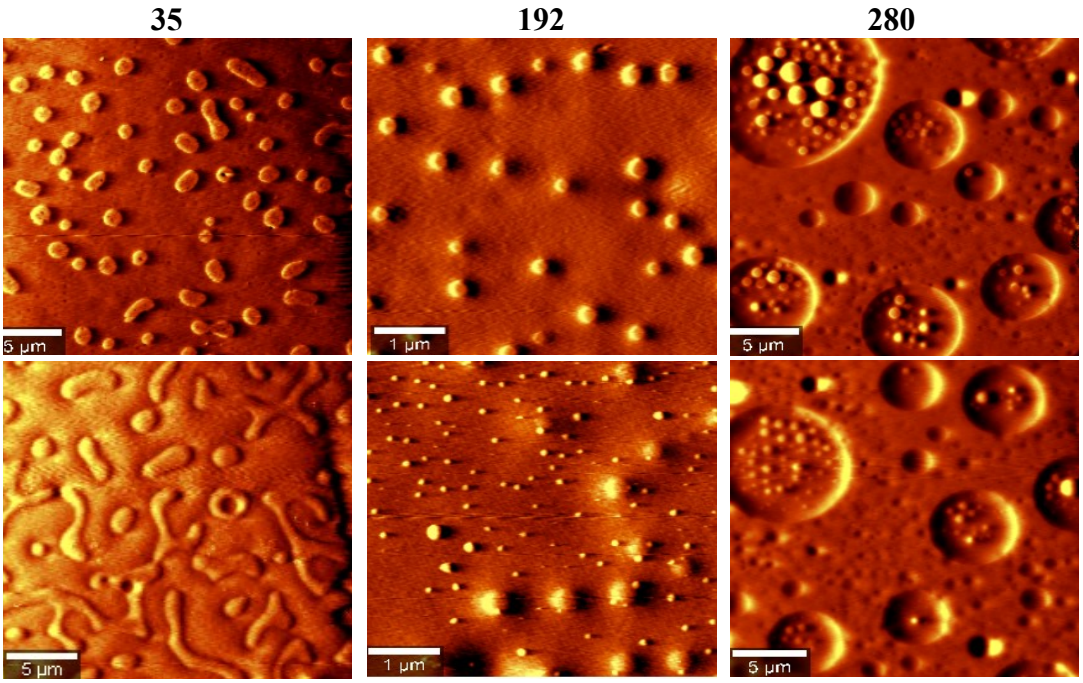

Figure 20. The effects of annealing at 160 ℃ for 30 minutes on 25:75 ratio blends of PS and PMMA using 3% concentrations. The molecular weights are denoted (factor 1/1000) on the image and varied from 35- 280. Top: surfaces after spin-coating; Bottom: after annealing.

The annealing process did not significantly alter the appearance of any of the polymer surfaces. In the case of the lowest molecular weight tested (i.e. MW=35), the features appear flattened and elongated, likely due to the increased diffusivity of the polymers. For the higher MWs, the surfaces were very similar between the annealed and un-annealed cases, as determined by AFM imaging. However, in the case of the use of a polymer brush layer, the changes to the surface were much more distinct (Figure 21).

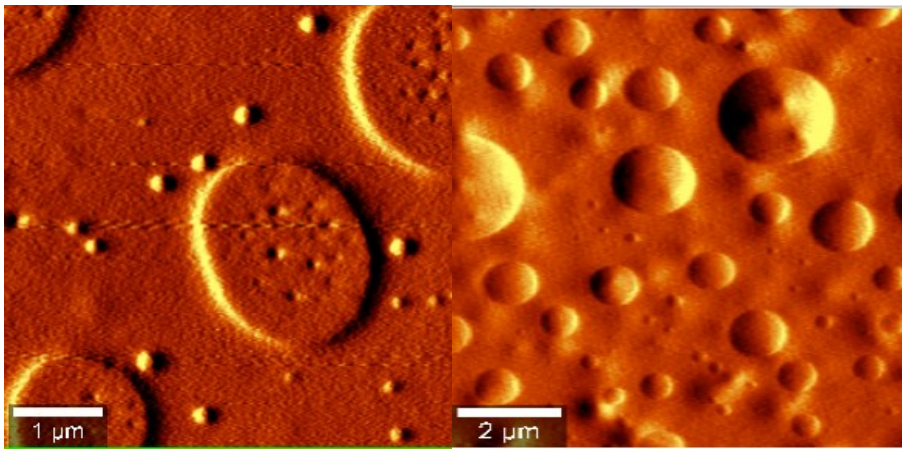

Figure 21. The effects of the use of a random brush layer tethered to the glass substrate prior to coating the PS:PMMA polymer blends. Left is a surface without brush and right is with the brush. The blend was composed of 25:75 192 MW PS to PMMA at 1% and annealed at 160 °C.

Polymer brushes are composed of differing monomers that are arranged randomly, and their use permits to minimize substrate interaction between the polymer and the glass to increase the order of the resulting surface topographical features [79, 80]. Figure 21 demonstrates that the introduction of the brush resulted in more uniform structures, albeit with a low degree of spatial order. Of note, the surface with the brush had less edging effects, such that all areas of the glass substrate showed the same topographical features.

Although varying the experimental conditions resulted in changes in the topographies of the polymer surfaces, there was no distinct and reproducible pattern that could be used to precisely investigate cell response to tailor-made surface structures. This can be attributed to the lack of equilibrium with mixing arising from the use of polymer blends rather than block copolymers. Similarly, as there is rapid evaporation occurring during the spin-coating process, the surfaces are likely richer in one polymer compared to the other. While the use of polymer blends does not pose any challenge, a valid alternative to tailor and fine-tune the morphologies is to use block copolymers. Block copolymers are composed of homopolymers that are linked to one another in a specific pattern at various junction points. When phase separation occurs in this

case, the morphologies that arise are still unique but have less variability due to the individual polymers being attached to each other [81, 82].

It was found that the variations of the experimental parameters (e.g. MW, composition and annealing temperature) did not impact the surface stiffness, a critical parameter known to affect cell activities (Figure 22) [16]. While the average stiffness varied across the concentration, the ratio of PS to PMMA, and the MW used, all of the results were statistically non-significant. However, it was noted that the use of a polymer brush was significant in increasing the stiffness of the polymer from 7.35 ± 0.44 N m^{-1} to 13.3 ± 1.7 N m^{-1}.

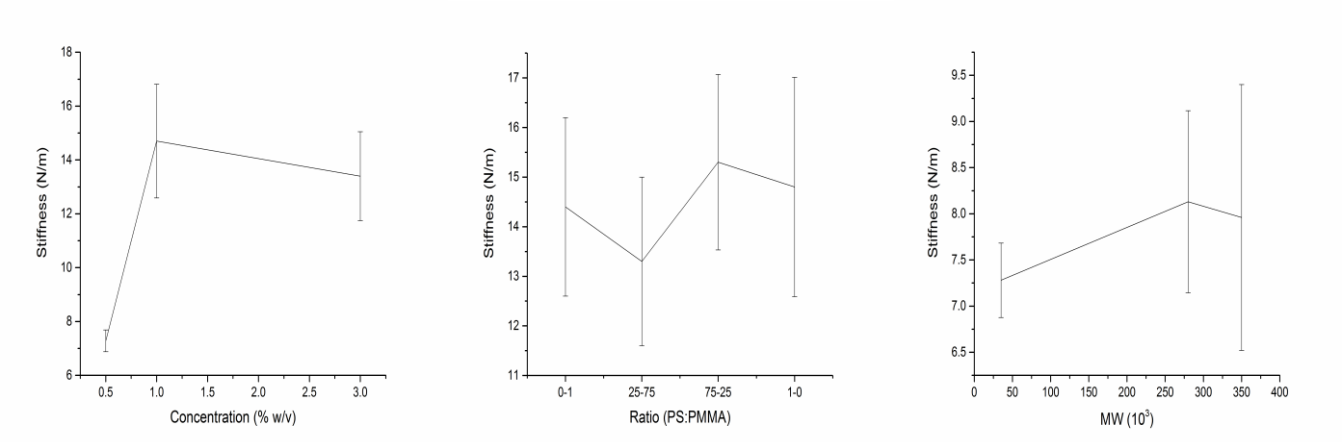

Figure 22. Stiffness variations as a function of the concentration, the ratio, and the molecular weight of the polymers used in the blends. Error bars denote standard deviation.

To investigate how neurons respond to micro/nano-topographical surfaces, three conditions that demonstrated high reproducibility were selected. These also had a wide range of features including small (<3 nm) dots, a combination of small and large (>3 nm) dots, and irregular features (Figure 23). As the surfaces evaluated in **Objective 1** did not have any distinct nano-features, it was of interest to determine whether the morphology of the underlying substrate could guide neuronal growth. Results from this study are poised to provide new insight into the

interactions with the extracellular matrix in the gastro-intestinal tract and ultimately guide the design of synthetic scaffolds to support their growth.

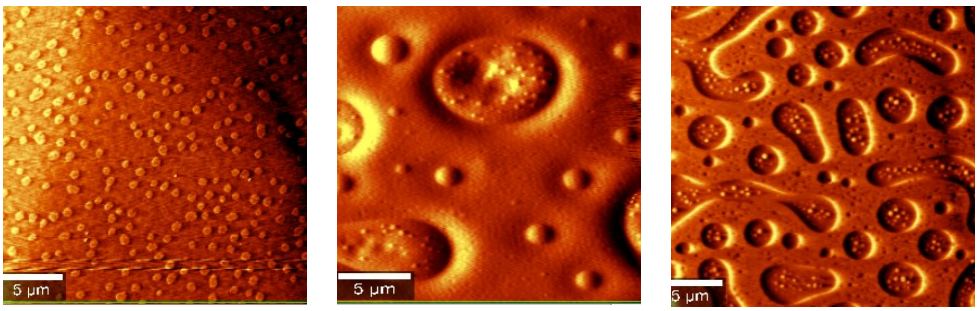

Figure 23. Three topography conditions selected to study enteric cell adhesion and viability. Left: 3% concentration, 35 kDa MW, 25:75 ratio. Middle: 1% concentration, 192 kDa MW, 50:50 ratio. Right: 1% concentration, 280 kDa MW, 25:75 ratio.

The size of the various features was measured by DPFM-AFM and analyzed by using the Witec® software. Values were averaged across 3 images per sample (10 µm X 10µm) for 3 replicates. These were namely the round nanodomains with negative height, round nanodomains with positive height, and cylindrical nanodomains with negative height. The features varied in diameter, from approximately 0.05 nm to 150 nm, and some projected from the substrate while others were cavities, offering different options to investigate neuronal adhesion and outgrowth. The height of the features varied from -138 nm to 15 nm. A summary of the range of sizes is shown in Table 3. It was also found that the stiffness of the aforementioned surfaces was uniform and did not vary depending on the feature type, indicating the mixing of the two polymers into a blend. Average stiffness values were averaged for each sample and were 13.4 N/m, 6.52 N/m, and 7.72 N/m for the 35 MW, 192 MW, and 280 MW conditions, respectively.

Table 3. Summary of feature width and height (± std dev) in nanometres on the surfaces shown in Figure 23.

Feature	Size (nm)	192 50:50 1%	280 25:75 1%	35 25:75 3%
Large circles	**Width**	8.12 ± 2.03	n/a	n/a
	Height	-123.69 ± 15.24		
Small circles	**Width**	2.79 ±0.87	2.64 ± 0.64	n/a
	Height	-49.08 ± 7.38	-30.35 ± 6.09	
Embedded circles within larger features	**Width**	0.69 ± 0.13	0.68 ± 0.27	1.62 ± 0.45
	Height	10.72 ± 2.33	11.17 ± 4.37	0.05 ± 0.001
Cylinders	**Width**	n/a	2.66 ± 0.80	n/a
	Height		-26.61 ± 3.85	

A limitation of the copolymer blends is that while there are no reports to indicate that they are toxic to cells, they were unable to support neuronal adhesion. This was overcome by functionalizing the polymer surface with polydopamine and laminin, in order to be able to bind the cells while allowing them to sense and detect the underlying features of the topography. At the same time, this allowed us the single out the effects of topography while keeping the surface chemistry consistent across different samples. The use of laminin was inspired from the results of **Objective 1**, but it was used without PDL in order to decrease the thickness of the coated layer. The chemical functionalization was verified using raman spectroscopy, Figure 24, and AFM. Raman is a means of measuring the chemical composition of a sample by shining a laser onto it. The laser interacts with the molecules in the sample and results in scattered light which is at a frequency that is different from the incident light and gives rise to a spectrum or chemical fingerprint [83, 84].

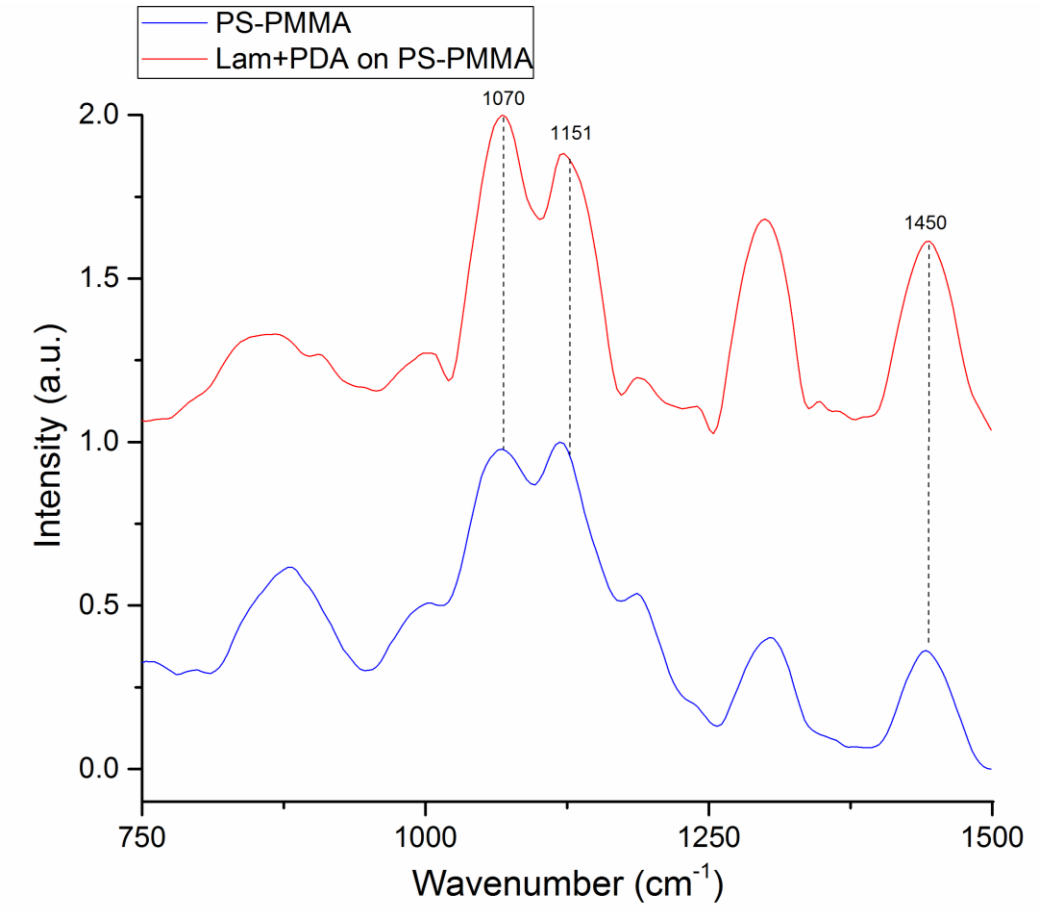

Figure 24. Plot of intensity against wavenumber obtained from Raman spectroscopy to evaluate effect of coating PS and PMMA with PDA and laminin. Spectra are offset for clarity.

Figure 24 shows peaks at 1151 cm^{-1} and 1450 cm^{-1} which represent the ester group and the angular deformation of C-H for PMMA, respectively [85, 86]. Notably, the peak at 1450 cm^{-1} shows an increase in magnitude in the condition with laminin, due to the introduction of an amide group [87]. In addition, there is a peak present at 1070 cm^{-1} as a result of the C-H flexion bond in polystyrene [88]. As seen above, all of the aforementioned peaks present in the PS-PMMA are retained in the laminin-functionalized condition, indicating that the thin protein layer did not mask the underlying surface. Additional peaks (unlabeled) appeared in 1200-1300 cm^{-1} range and are attributed to the presence hydroxyl and aldehyde bonds in the underlying PDA [72]. This was additionally confirmed with contact images obtained using atomic force

microscopy (not shown), as the surfaces of both the functionalized and un-functionalized polymers appeared identical.

4.2 Neuronal adhesion to polymer blend surfaces

The addition of the PDA and laminin layer promoted the adhesion of the enteric neurons to the polymers, which was evaluated as previously described in **Objective 1** and which can be seen in Figure 25.

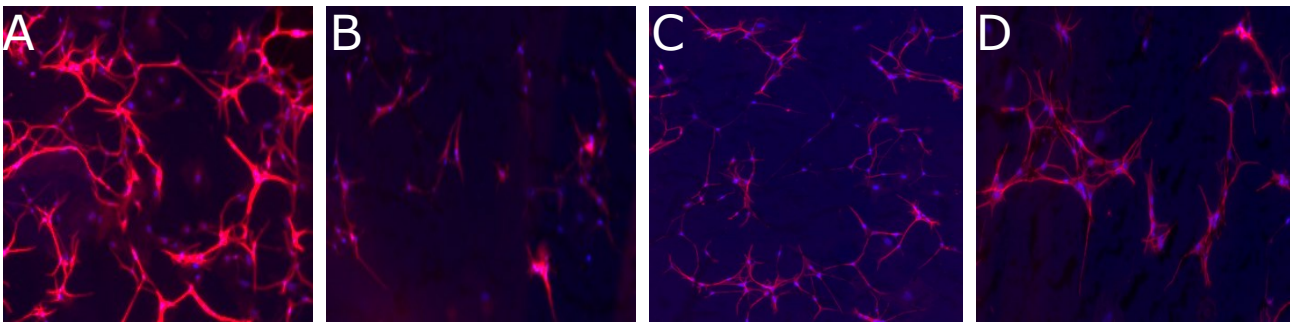

Figure 25. Immunofluorescence binding of the neurons on substrates: A. glass, B. 25:75 280 MW PS:PMMA at 1% w/v and annealed, C. 50:50192 MW PS:PMMA at 1% w/v and annealed with a brush layer, D. 25:75 35 MW PS:PMMA at 3% w/v and annealed.

It was visually evident that the density of neurons was higher on the glass surface compared to the polymer blends, but similar to results that were observed on the laminin and PDL condition in **Objective 1.** This was confirmed by measuring the percentage surface area of the images that were covered with either neurons or neurites, shown below. The ability of the three blends to support neuronal adhesion and viability was statistically non-significant between one another, but substantially less than that of functionalized glass. This indicated that the copolymer topographies were equal in serving as a platform for the neurons but that the cells preferred the smoother glass surface. As all of the surfaces were quite uniform, it is unlikely that the pattern or arrangement of the topographical features were an impediment to the neurons, but rather the roughness of the surface compared to glass. Amongst the polymers, the most neurite

outgrowth was seen on the 35 MW condition which had the smallest sized features. This suggests that the size of the topographical attributes may have played a contributing factor, as many of them were larger than what the cells would be exposed to in the gastrointestinal tissue.

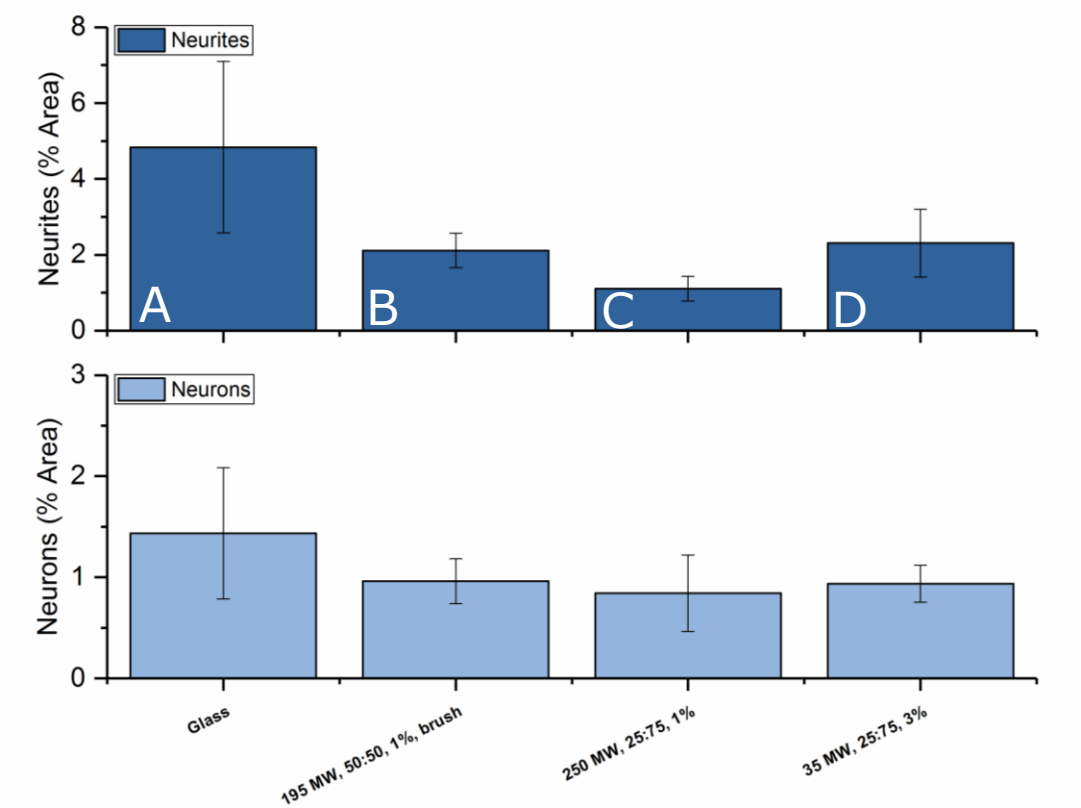

Figure 26. Number of neurons and neurites bound to the polymer blends functionalized with laminin, calculated as a percentage of the surface area of the images analyzed. Ten images collected across 3 samples were averaged using ImageJ software. Error bars denote standard deviation.

As in **Objective 1,** an additional analysis was performed to relate the neurite outgrowth to the number of neurons as a means of determining whether certain topographies stimulate neurite outgrowth from each neuron more than others. Figure 27 shows an averaged value of neurites for each neuron on the surface of the polymers but all of the results were found to be statistically non-significant at $p<0.05$. Accordingly, only the percentage surface area of the neurons and neurites was utilized for analysis.

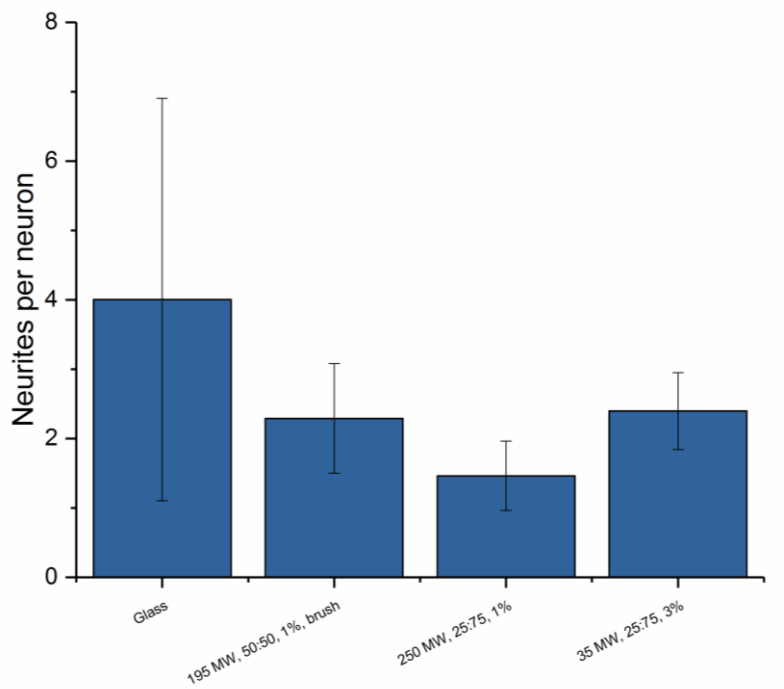

Figure 27. Averaged number of neurites per neuron for the functionalized polymers and glass used to support enteric neurons. The results are statistically non-significant across all conditions as determined with ANOVA at $p<0.05$.

While the immunofluorescence images can provide insight on the number of cells adhering to the polymers, it does not allow us to conceive the nature of the interactions. Thus, scanning electron microscopy was employed to produce an image of the neurons and the polymers' topographical features. SEM allows for visualization of a sample by scanning its surface with a beam of electrons. These will interact with the atoms in the sample and cause various signals and electron emission which can be collected and compiled to generate an image [89]. SEM was performed on the three aforementioned conditions and on glass; samples of the results are shown below.

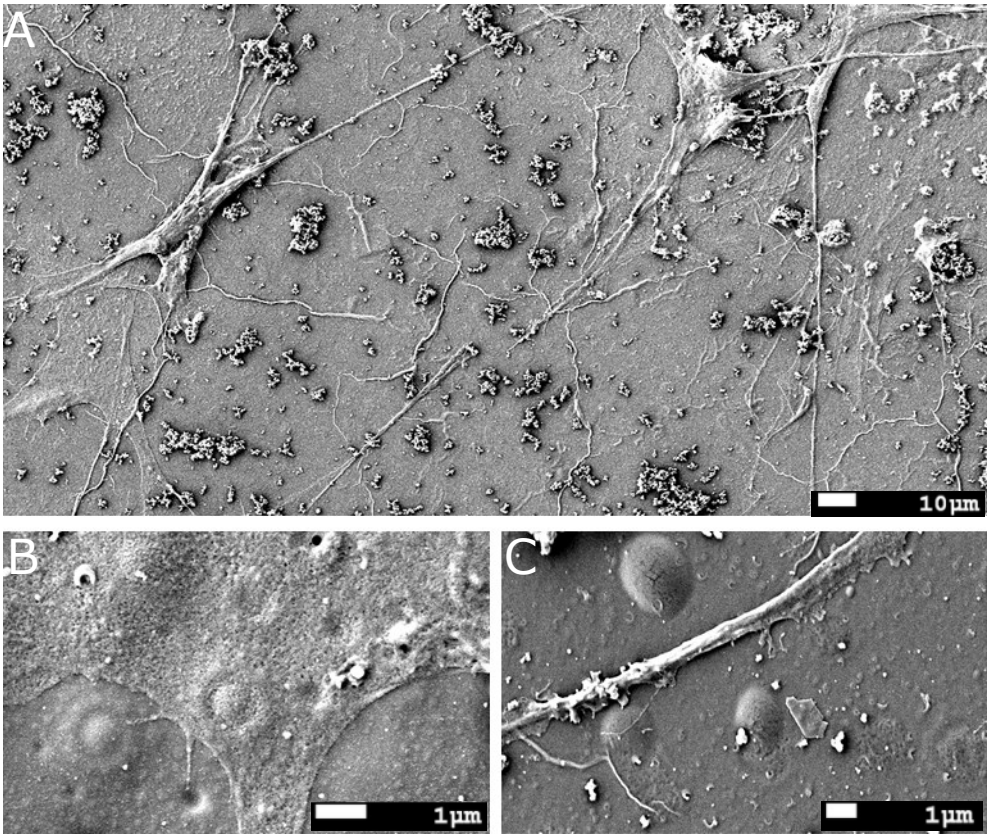

Figure 28. Scanning electron microscopy images of enteric neurons cultured for 9 days, onto polymeric coatings that were functionalized with PDA and laminin. A. Neurons on 192 MW, 50:50 ratio sample using 400X magnification and 17 mm working distance. B. Magnified portion of image in A taken at 5000X magnification showing cell body. C. Magnified potion of image in A taken at 3000X magnification showing neurite. Debris shown on the surface are PDA aggregates resulting from dopamine polymerization.

As seen above, the enteric neurons were found to bind to the topographical features of the surfaces regardless of their size or shape. Insert A of Figure 28 shows a larger view of the neurons on the 192 MW condition. The neurite networks are not as complex as those that were observed with immunofluorescence in **Objective 1**, but the neurons were able to bind to the surface and experience extensive neurite outgrowth. The neurons conformed to the structures, as seen in B, in cases when they were both protruding and sunken. The large granular crystals visible on the surface are aggregates of polydopamine which are present underneath the laminin coating. It was also observed (Figure 28-C) that the neurites followed pathways that avoided

interaction with larger surface features. However, the interactions observed were not sufficient to be able to extrapolate a pattern as the neurons both avoided and adhered to the topographical features. Based on the results above, the glass substrate was selected for use in **Objective 3** studies.

Chapter 5- Objective 3: Results and Discussion

In addition to topography and stiffness, cells respond to changes in their chemical environment through a process known as chemotaxis. Chemotaxis is particularly important during neurite growth and migration as growth cones are directed by responding to attractive or repulsive chemical signals. Similarly, cellular migration plays a critical role in pathological processes, thus understanding the mechanisms that drive neurite outgrowth and movement is critical for better studying gastro-intestinal related diseases. While there have been many studies trying to gain further insight into the topic in relation to cortical neurons, there is limited knowledge of how chemical signals influence enteric neurons [50, 90].

In this context, **Objective 3** of this work served to elucidate how enteric neurons respond to changes in protein concentration by employing microfluidic techniques. Microfluidic systems are PDMS and silicon based devices which handle small quantities of fluids [91]. For this application, a PDMS chip with a Y-shaped channel was used to generate a linear gradient of laminin onto PDA coated glass using tools and methodology developed by the Biomimetic Systems for Cell Engineering group at the Institute of Bioengineering of Catalonia [54]. This approach maintains the properties which were selected based on **Objectives 1 and 2** like the surface coating, while varying the intrinsic length scale, or slope, of the gradient such that concentration is not uniform across the surface.

The method employed created a gradient that ranged from 0 to 20 ug mL^{-1} and matched the concentration of protein that was used to coat the surfaces described in **Objectives 1 and 2.** A fluorescence image of the protein on the glass surface is shown in Figure 29.

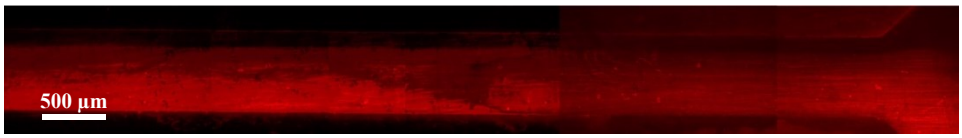

Figure 29. Fluorescence image of protein gradient formed using the Y-shaped channels in the microfluidic chip. Laminin is diluted with PBS to aid in the formation of a linear concentration profile. Laminin concentration increases from top to bottom.

As it is not possible to image the entire length of substrate, the image above is a rendering of multiple photographs, each representing a segment of the gradient. Accordingly, there are some discontinuities but a change in fluorescence intensity can be visualized in the perpendicular direction, with a higher intensity indicative of a higher protein concentration. This change in intensity across the surface is quantified in the graph below.

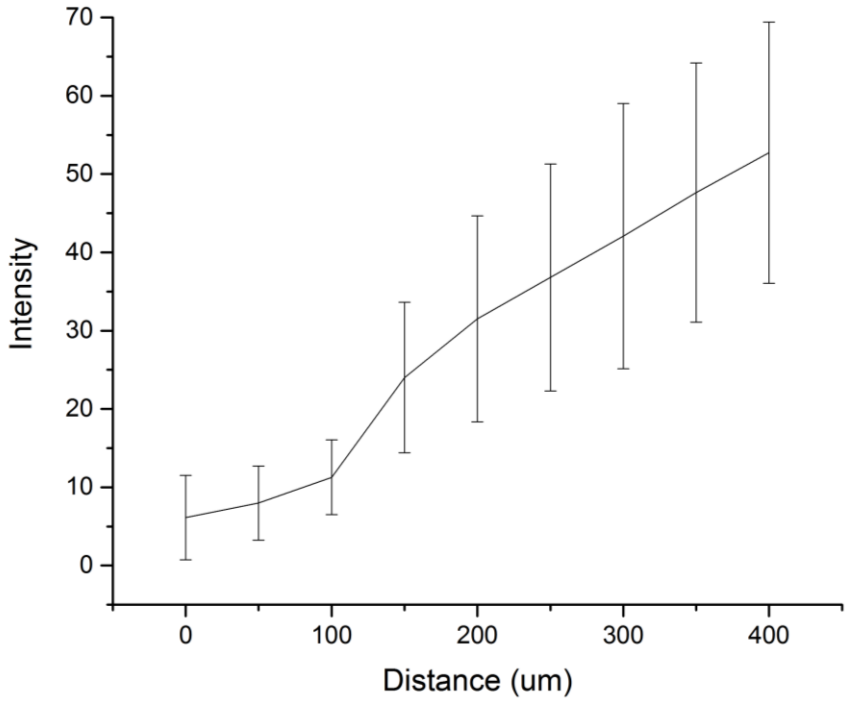

Figure 30. Plot of fluorescence intensity (arbitrary units) of laminin protein against distance generated using microfluidic techniques.

The protein gradient is generated by using syringe pumps to deliver fluid through the microfluidic chip. In order to ensure exact linearity of the gradient, both pumps must run simultaneously and cannot have any timing discrepancies. However, as the pumps are turned on

manually, it is difficult to avoid offsets in time. This factor may account for the large range of variability in the plot above, as it is the average of three trials.

The enteric neurons were cultured onto a substrate with a laminin gradient and onto a substrate with a uniform laminin coating, to compare their response and migration to a varied concentration profile. The cells were placed in a live imaging system one day after culture, and a photo was taken every 30 minutes over the course of the next 48 hours. Each image covered a 3400x2550 μm area of the surface. Figure 31 shows the movement of neurons across the same plane over the course of 48 hours on a sample without gradient.

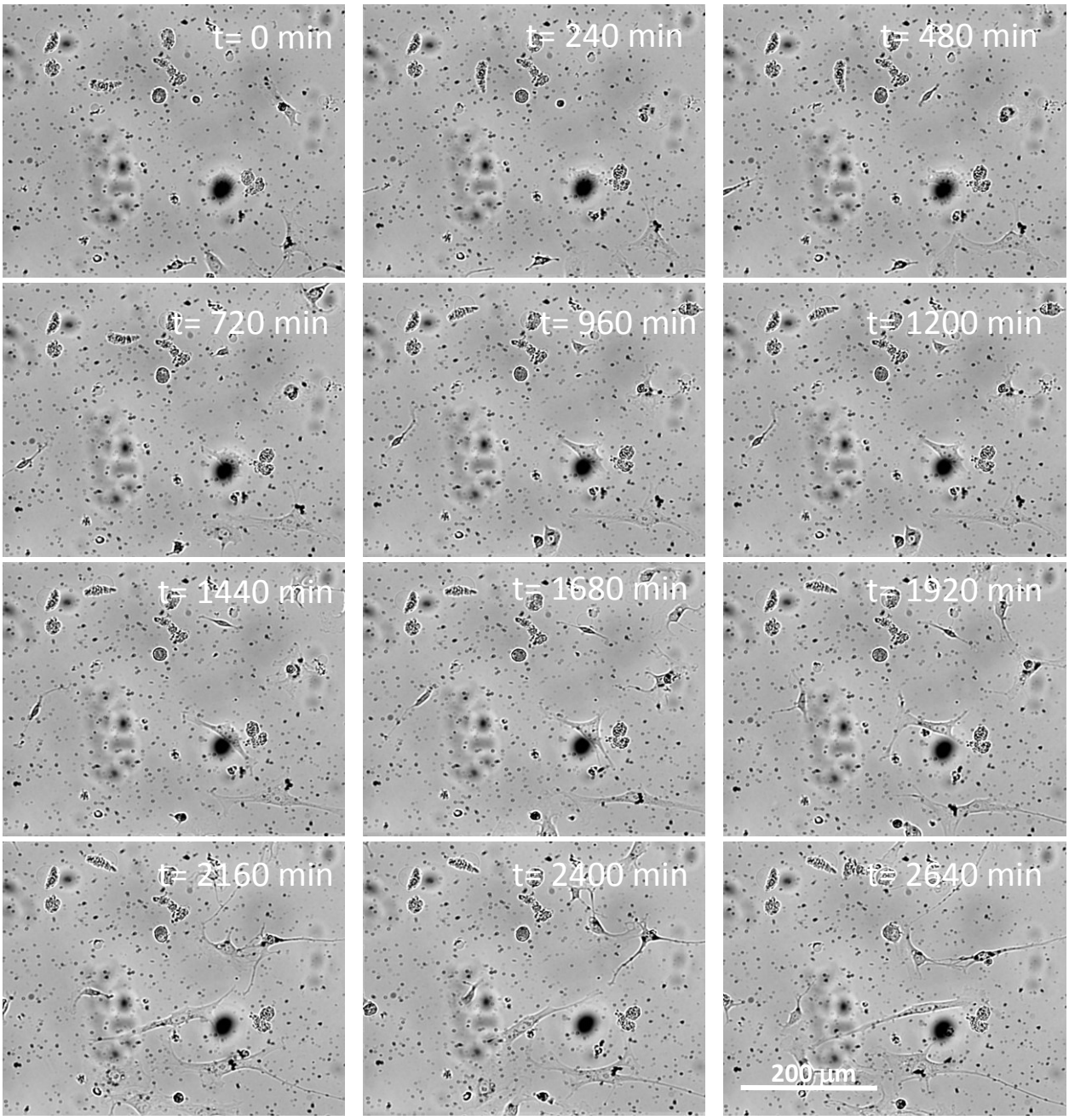

Figure 31. Phase contrast images taken at 10X magnification of neurons cultured onto a glass slide coated with dopamine and a uniform concentration of laminin across the surface (no gradient). Images were taken over the course of 48 hours and represent a 420x312 µm surface. The small black dots are dopamine aggregates, while the larger ones are artifacts present on the surface of the microscope objective.

In the first 4 hours of imaging, it can be observed that there was very little neurite extension and the neurons remained fairly stationary. However, after 24 hours, the neurons began

to move across the substrate's surface while using their neurites as guides. The cells appear to adhere their neurites to the polydopamine aggregates and use them as pivot points. This may be attributed to a possible increased firmness of these aggregates compared to the rest of the fairly smooth surface and offers a route to explore in further studies.

While Figure 31 suggests that the neurons travelled primarily towards the left, the images shown above are taken from a small area (0.13 mm^2) from a much larger image (8.67 mm^2). Accordingly, the directionality of the neurons observed is not representative of the entire surface. A more characteristic map of neuron trajectories averaged from across the surface is shown in Figure 32.

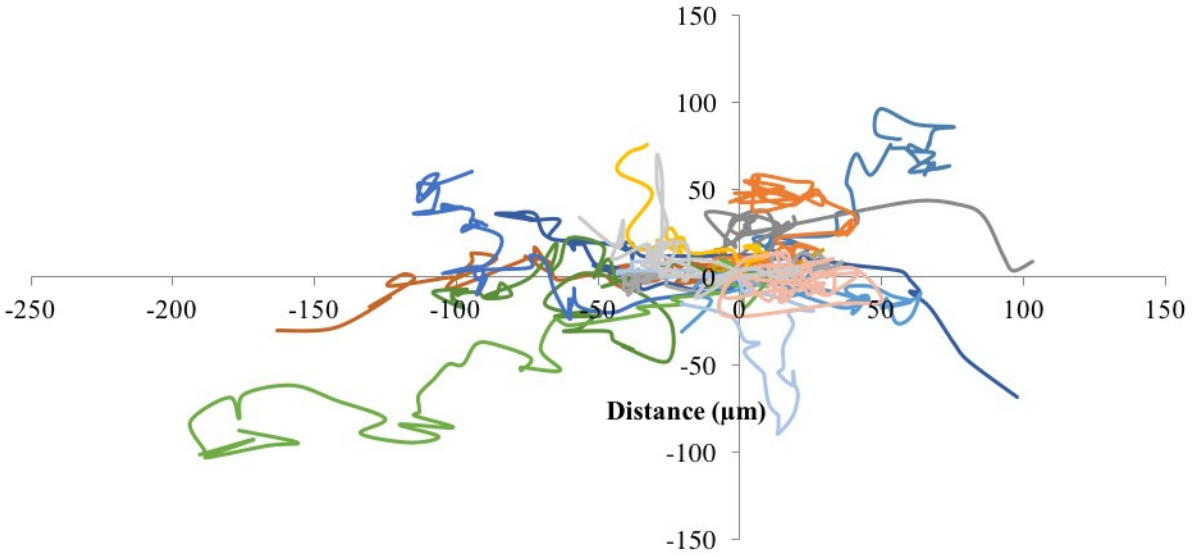

Figure 32. The trajectories of 15 neurons over 48 hours and their distance travelled (µm) in the x and y direction normalized to their respective start points.

The movement of the neurons on the surface was fairly random and they did not appear to demonstrate a strong preference to any particular area. This result is expected as the concentration of laminin on the surface of the substrate was uniform, thus there was no signal to direct the motion of the neurons. While a majority, 31%, of the cells migrated towards the left,

this number was not large enough to indicate a deliberate response. A summary of the directionality of the cells is found in Table 4.

Table 4. Summary of direction of motion of the neurons cultured on substrate coated with dopamine and a uniform concentration of laminin (no gradient). The percentage of cells is based on 40 which were observed on a 0.8 mm^2 area.

Direction	Cells (%)
Upwards and right	17
Upwards and left	22
Downwards and left	31
Downwards and right	19
Left only	5
Down only	3
No change	3

As noted previously, there appears to be some preference towards downwards and left motion on the substrate, however, this value does not take into account the distance travelled. When observed in conjunction with Figure 32, it is seen that many of the cells did not travel large distances and remained fairly centered around their initial position. While these results are consistent with expectations, the experiment will need to be repeated to add statistical certainty.

The neurons were then cultured on a substrate coated with dopamine and a linear concentration gradient of laminin. These cells were too cultured for 24 hours prior to being placed in a live imaging system. However, due to technical malfunctions of the Zeiss AxioObserver-Z1, significant cell loss was encountered and imaging could not be completed. It is anticipated that the cells would migrate towards the higher protein concentration area of the

substrate and similarly that neurite length would be longest in this region [92]. In addition, it is likely that some of the neurons would align themselves in the direction of the gradient.

It is a primary priority to complete this study in order to further our understanding of signalling and chemotaxis in enteric neurons. Many gastrointestinal disorders are characterized by either a complete lack of neurons, or their scarcity. Accordingly, in order to design effective regenerative therapies, it is critical to be able to not only stimulate the outgrowth of neurites but also to be able to guide the directionality of their movement [93]. In addition, the protein gradient may be combined with physical gradients (such as stiffness) to provide a more realistic model of the gastrointestinal environment and elucidate any synergistic effects to be able to provide a starting point for the development of neuro-regenerative scaffolds [94].

Chapter 6- Future Work

The aim of this work was to further the current knowledge of the ENS with the goal of being able to develop successful interventions to improve the treatment of gastro-intestinal diseases in children. While the results described have provided valuable insight, work remains to be completed to achieve this research goal.

The methodology that was developed to study neuron electrophysiology on MEAs will be applied to look at the effect of drug treatments on disorders of the gut. Intestinal tissue samples obtained from patients at CHEO will be treated as described in **Objective 1** in an effort to standardize care plans. This method will optimize drug selections for these patients by maximizing effectiveness without subjecting them to unwanted side-effects which could occur if they were to test drug treatments on their own.

In addition, the experiments which could not be completed in support of **Objective 3** will be repeated to evaluate the effect of a linear gradient on neuron motility and neurite outgrowth. Further, the gradient will be applied in conjunction with the unique nanotopographies to be designed using block copolymers in order to recreate the gastrointestinal environment as closely as possible. Results from these experiments will combined with additional work currently being performed by CHEO to convert stem cells into enteric neurons, in order to develop scaffolds which can be implanted into diseased intestinal tissue. The scaffolds will be seeded with neurons and coated with a gradient to stimulate outgrowth from surrounding areas with the goal of introducing and supporting neurons in areas of the intestine from which they may be absent. In addition, there are currently mouse models for diseases such as Parkinson's, Rett's, and Hischprungs which aid to facilitate the research of this type of method.

This type of work will be particularly useful for disorders characterized by the absence of enteric neurons, such as Hirschprung's. Currently, treatments are aimed at minimizing symptoms rather than eliminating them, and a tissue engineering approach would provide a more permanent solution.

Chapter 7- Conclusions

The first part of this work intended to evaluate various polymers used in biomedical applications to determine which would be capable of supporting neuron adhesion and neurite growth on a glass substrate. While the enteric neurons had been previously cultured onto plastic, attempts on glass were unsuccessful and presented a barrier in being able to study electrophysiology on multichannel electrode arrays. Matrigel® was most the most efficacious at promoting both neuron adhesion and neurite outgrowth but it acted as an insulating material. Thus, laminin protein and poly-d-lysine coated onto polydopamine were applied to be able to measure neuron dynamics. The use of polydopamine was found to be essential in ensuring the stability of the laminin and poly-d-lysine on the glass substrate which would otherwise dissolve into the cell media.

The same coating was also used to functionalize the surface of blends of poly(styrene) and poly(methyl methacrylate) which were spin coated onto glass, to be able to elucidate the effects of nanotopography on enteric neuron behavior. Three distinct surfaces were used as cell culture platforms and were compared to functionalized glass as a reference. Out of the three blends tested, it was found that the neurons preferentially bound to the substrate which had the smallest topographical features, however, not in as high numbers as they bound to the glass. It cannot be concluded that the neurons prefer smoother topography as the features of the polymer blends were larger than what the cells would typically be exposed to in the gastrointestinal tract. Therefore, future work will involve the use of block copolymers rather than polymer blends as their topographical features can be more readily fine-tuned. This will allow for the design of cell culture platforms that mimic the internal environment the neurons are exposed to *in-vivo*.

It was also shown that neuronal motion on a uniform substrate is randomized and does not travel preferentially in any particular direction. The neuronal response on a uniform concentration of protein was intended to be compared to that on a linear chemical gradient; however, technical shortcomings hindered this analysis. The results to date provide meaningful insight as a starting point for future studies that will complete the intended experiment. It is expected that the neurons will primarily extend their neurites in the direction of higher protein concentration. In addition, the gradient will be applied in conjunction with the unique nanotopographies to be designed using block copolymers in order to recreate the gastrointestinal environment as closely as possible.

In summary, this Thesis fine-tuned a novel protocol for the culture of enteric neurons and developed a method to be able to study the electrophysiology of the ENS. It also presented insight into the fundamental interactions of neurons with surfaces of varying topographies and mechanical properties. It is our hope that the results and future work will be used to broaden our knowledge of the ENS and its relation to enteric diseases, ultimately leading to the development of novel polymeric scaffolds to replace enteric neurons in the gut.

Works Cited

1. Costa M, Brookes SJH, Hennig GW (2000) Anatomy and physiology of the enteric nervous system. Gut 47:15–19.

2. Furness JB (2012) The Enteric Nervous System and Neurogastroenterology. Nat Rev Gastroenterol Hepatol 9:286–294.

3. Avetisyan M, Schill EM, Heuckeroth RO (2015) Building second brain in bowel. Journal of Clinical Investigation 125:899–907.

4. Nezami BG, Srinivasan S (2013) Enteric Nervous System in the Small Intestine: Pathophysiology and Clinical Implications. Curr Gastroenterol Rep 12:358–365. doi: 10.1007/s11894-010-0129-9.Enteric

5. Lake JI, Heuckeroth RO (2013) Enteric nervous system development: migration, differentiation, and disease. AJP: Gastrointestinal and Liver Physiology 305:G1–G24. doi: 10.1152/ajpgi.00452.2012

6. Smith TH, Ngwainmbi J, Grider JR, Dewey WL, Akbarali HI (2013) An In-vitro Preparation of Isolated Enteric Neurons and Glia from the Myenteric Plexus of the Adult Mouse. Journal of Visualized Experiments 1–8. doi: 10.3791/50688

7. Hansen MB (2003) The enteric nervous system I: organisation and classification. Pharmacology & toxicology 92:105–113. doi: 10.1034/j.1600-0773.2003.t01-1-920301.x

8. Kenny SE, Chhabra S (2016) Hirschsprung ' s disease. Surgery 34:628–632. doi: 10.1016/j.mpsur.2016.10.002

9. Sasselli V, Pachnis V, Burns AJ (2012) The enteric nervous system. Developmental Biology 366:64–73. doi: 10.1016/j.ydbio.2012.01.012

10. Uranga-Ocio JA, Bastús-Díez S, Delkáder-Palacios D, García-Cristóbal N, Leal-García MÁ, Abalo-Delgado R (2015) Enteric neuropathy associated to diabetes mellitus. Revista espanola de enfermedades digestivas : organo oficial de la Sociedad Espanola de Patologia Digestiva 107:366–73.

11. Wahba G, Hebert A, Grynspan D, Staines W, Schock S (2016) A rapid and efficient method for dissociated cultures of mouse myenteric neurons. Journal of Neuroscience Methods 261:110–116. doi: 10.1016/j.jneumeth.2015.11.024

12. Derkinderen P, Rouaud T, Lebouvier T, Neunlist M, Giorgio R De (2011) Parkinson disease The enteric nervous system spills its guts. Neurology 77:1761–1767.

13. Frye RE, Rose S, Slattery J, Macfabe DF, Frye RE, Rose S, Slattery J, Macfabe DF, Macfabe DF (2015) Gastrointestinal dysfunction in autism spectrum disorder: the role of the mitochondria and the enteric microbiome. Microbiol Ecology in Health and Disease. doi: 10.3402/mehd.v26.27458

14. Wahba G, Schock SC, Claridge E, Bettolli M, Grynspain D, Humphreys P, Staines W (2015) MeCP2 in the enteric nervous system. Neurogastroenterol Motil 27:1156–1161. doi: 10.1111/nmo.12605

15. Yu LMY, Leipzig ND, Shoichet MS (2008) Promoting Neuron Adhesion and Growth. Materials Today 11:36–43.

16. Balgude AP, Yu X, Szymanski A, Bellamkonda R V. (2001) Agarose gel stiffness determines rate of DRG neurite extension in 3D cultures. Biomaterials 22:1077–1084. doi: 10.1016/S0142-9612(00)00350-1

17. Kamm M a (2000) Why the enteric nervous system is important to clinicians. Gut 47 Suppl 4:iv8-9; discussion iv10.

18. Belkind-gerson J, Graeme-cook F, Winter H (2006) Enteric Nervous System Disease and Recovery , Plasticity , and Regeneration. Journal of Pediatric Gastroenterology and Nutrition 42:343–350.

19. Theocharis AD, Skandalis SS, Gialeli C, Karamanos NK (2016) Extracellular matrix structure ☆. Advanced Drug Delivery Reviews 97:4–27. doi: 10.1016/j.addr.2015.11.001

20. Rao M, Gershon MD (2016) The bowel and beyond : the enteric nervous system in neurological disorders. Nature Publishing Group 13:517–528. doi: 10.1038/nrgastro.2016.107

21. Lodish H, Berk A, Zipursky S (2000) Molecular Cell Biology, 4th ed. W.H. Freeman, New York

22. Brunet T, Arendt D (2016) From damage response to action potentials: early evolution of neural and contractile modules in stem eukaryotes. Philosophical transactions of the Royal Society of London Series B, Biological sciences 371:20150043-. doi: 10.1098/rstb.2015.0043

23. Barnett MW, Larkman PM (2007) The action potential. Pract Neurol 7:192–197. doi: 10.1007/978-3-319-26197-3_3

24. Mumba JM, Mumba JM, Kasandji F (2017) Pharmacology of Local Anaesthetics and Commonly Used Recipes in Clinical Practice. In: Current Topics in Anesthesiology. InTech, pp 3–22

25. Bean BP (2007) The action potential in mammalian central neurons. Nature Reviews Neuroscience 8:451–465. doi: 10.1038/nrn2148

26. Amin AS, Tan HL, Wilde AAM (2010) Cardiac ion channels in health and disease. Heart Rhythm 7:117–126. doi: 10.1016/j.hrthm.2009.08.005

27. Cooper EC, Jan LY (1999) Ion channel genes and human neurological disease: Recent progress, prospects, and challenges. Proc Natl Acad Sci U S A 96:4759–4766. doi:

10.1073/pnas.96.9.4759

28. Rakhilin N, Barth B, Choi J, Muñoz NL, Kulkarni S, Jones JS, Small DM, Cheng Y-T, Cao Y, LaVinka C, Kan E, Dong X, Spencer M, Pasricha P, Nishimura N, Shen X (2016) Simultaneous optical and electrical in vivo analysis of the enteric nervous system. Nature Communications 7:11800. doi: 10.1038/ncomms11800

29. Spira ME, Hai A (2013) Multi-electrode array technologies for neuroscience and cardiology. Nature Nanotechnology 8:83–94. doi: 10.1038/nnano.2012.265

30. Russell JT (2011) Imaging calcium signals in vivo: A powerful tool in physiology and pharmacology. British Journal of Pharmacology 163:1605–1625. doi: 10.1111/j.1476-5381.2010.00988.x

31. Scanziani M, Häusser M (2009) Electrophysiology in the age of light. Nature 461:930–939. doi: 10.1038/nature08540

32. Obien MEJ, Deligkaris K, Bullmann T, Bakkum DJ, Frey U (2015) Revealing neuronal function through microelectrode array recordings. Frontiers in Neuroscience 9:423. doi: 10.3389/fnins.2014.00423

33. Hales CM, Rolston JD, Potter SM (2010) How to Culture, Record and Stimulate Neuronal Networks on Micro-electrode Arrays (MEAs). Journal of Visualized Experiments 1–7. doi: 10.3791/2056

34. Kelly RC, Smith MA, Samonds JM, Kohn A, Bonds AB, Movshon JA, Sing Lee T (2007) Comparison of Recordings from Microelectrode Arrays and Single Electrodes in the Visual Cortex. Journal of Neuroscience 27:261–264. doi: 10.1523/JNEUROSCI.4906-06.2007

35. Multichannel Systems (2014) Microelectrode array (MEA) manual. 1–131.

36. Raghavan S, Gilmont RR, Bitar KN (2013) Biomaterials Neuroglial differentiation of adult enteric neuronal progenitor cells as a function of extracellular matrix composition. Biomaterials 34:6649–6658. doi: 10.1016/j.biomaterials.2013.05.023

37. Pelham JRJ and WY-L (1998) Cell locomotion and focal adhesions are regulated by substrate flexibility. Proc Natl Acad Sci USA 94:13661–13665. doi: 10.1073/pnas.94.25.13661

38. Engler A, Sheehan M, Sweeney HL, Discher DE (2003) Substrate compliance vs ligand density in cell on gel responses. European Cells and Materials 6:7–8. doi: 10.1016/S0006-3495(04)74140-5

39. Alves NM, Pashkuleva I, Reis RL, Mano JF (2010) Controlling cell behavior through the design of polymer surfaces. Small 6:2208–2220. doi: 10.1002/smll.201000233

40. Zhou L, Cai M, Tong T, Wang H (2017) Progress in the Correlative Atomic Force

Microscopy and Optical Microscopy. Sensors 17:938. doi: 10.3390/s17040938

41. Heinisch JJ, Lipke PN, Beaussart A, El Kirat Chatel S, Dupres V, Alsteens D, Dufrene YF (2012) Atomic force microscopy - looking at mechanosensors on the cell surface. Journal of Cell Science 125:4189–4195. doi: 10.1242/jcs.106005

42. Ton-That C, Shard AG, Bradley RH (2002) Surface feature size of spin cast PS/PMMA blends. Polymer 43:4973–4977. doi: 10.1016/S0032-3861(02)00333-6

43. Ahn DU, Wang Z, Campbell IP, Stoykovich MP, Ding Y (2012) Morphological evolution of thin PS/PMMA films: Effects of surface energy and blend composition. Polymer (United Kingdom) 53:4187–4194. doi: 10.1016/j.polymer.2012.07.037

44. Li X, Han Y, An L (2004) Annealing effects on the surface morphologies of thin PS/PMMA blend films with different film thickness. Applied Surface Science 230:115–124. doi: 10.1016/j.apsusc.2004.02.046

45. Roy S, Sharma A (2015) Self-organized morphological evolution and dewetting in solvent vapor annealing of spin coated polymer blend nanostructures. Journal of Colloid and Interface Science 449:215–225. doi: 10.1016/j.jcis.2014.12.095

46. Prosycevas I, Tamulevicius S, Guobiene A (2004) The surface properties of PS/PMMA blends nanostructured polymeric layers. Thin Solid Films 453–454:304–311. doi: 10.1016/j.tsf.2003.11.090

47. van Midwoud PM, Janse A, Merema MT, Groothuis GM, Verpoorte E (2012) Comparison of biocompatibility and adsorption properties of different plastics for advanced microfluidic cell and tissue culture models. Anal Chem 84:3938–3944. doi: 10.1021/ac300771z [doi]

48. de Melo Â, Bet AC, Assreuy J, Debacher NA, Soldi V (2009) Adhesion of L929 mouse fibroblast cells on poly(styrene)/poly(methyl methacrylate) films. Journal of the Brazilian Chemical Society 20:1753–1757. doi: 10.1590/S0103-50532009000900026

49. Troemel ER, Kimmel BE, Bargmann CI (1997) Reprogramming chemotaxis responses: Sensory neurons define olfactory preferences in C. elegans. Cell 91:161–169. doi: 10.1016/S0092-8674(00)80399-2

50. Rao Y, Wong K, Ward M, Jurgensen C, Wu JY (2002) Neuronal migration and molecular conversation with leukocyte chemotaxis. Genes Dev 16:2973–2984. doi: 10.1101/gad.1005802.migrate

51. Georgescu W, Jourquin J, Estrada L, Anderson ARA, Quaranta V, Wikswo JP (2008) Model-controlled hydrodynamic focusing to generate multiple overlapping gradients of surface-immobilized proteins in microfluidic devices. Lab Chip 8:238–244. doi: 10.1039/B716203K

52. Kilic O, Pamies D, Lavell E, Schiapparelli P, Feng Y, Hartung T, Bal-Price A, Hogberg

HT, Quinones-Hinojosa A, Guerrero-Cazares H, Levchenko A (2016) Brain-on-a-chip model enables analysis of human neuronal differentiation and chemotaxis. Lab Chip 16:4152–4162. doi: 10.1039/C6LC00946H

53. Fishell G, Mason CA, Hatten ME (1993) Dispersion of neural progenitors within the germinal zones of the forebrain. Nature 362:636–638.

54. Pujadas JC (2012) Biochemical gradients on Poly(methylmethacrylate) surfaces. Universitat de Barcelona

55. Roduit C, Sekatski S, Dietler G, Catsicas S, Lafont F, Kasas S (2009) Stiffness tomography by atomic force microscopy. Biophysical Journal 97:674–677. doi: 10.1016/j.bpj.2009.05.010

56. Galligan JJ (1999) Nerve Terminal Nicotinic Cholinergic Receptors on Excitatory Motoneurons in the Myenteric Plexus of Guinea Pig Intestine 1. 291:92–98.

57. Andrade F, Goycoolea F, Chiappetta DA, Sosnik A, Sarmento B (2011) as Matrices for Pulmonary Drug Delivery. doi: 10.1155/2011/865704

58. Muzzarelli RAA (2009) Genipin-crosslinked chitosan hydrogels as biomedical and pharmaceutical aids. Carbohydrate Polymers 77:1–9. doi: 10.1016/j.carbpol.2009.01.016

59. Nirasay S, Badia A, Leclair G, Claverie JP, Marcotte I (2012) Polydopamine-Supported Lipid Bilayers. 2621–2636. doi: 10.3390/ma5122621

60. Chuah YJ, Koh YT, Lim K, Menon N V, Wu Y, Kang Y (2015) Simple surface engineering of polydimethylsiloxane with polydopamine for stabilized mesenchymal stem cell adhesion and multipotency. Nature Publishing Group 1–12. doi: 10.1038/srep18162

61. Amrani S, Variola F (2015) Modulating the elution of antibiotics from nanospongy titanium surfaces with a pH-sensitive. RSC Advances 5:93666–93675. doi: 10.1039/C5RA18296D

62. Gao L, Gan H, Meng Z, Gu R, Wu Z, Zhang L, Zhu X, Sun W, Li J, Zheng Y, Dou G (2014) Colloids and Surfaces B : Biointerfaces Effects of genipin cross-linking of chitosan hydrogels on cellular adhesion and viability. Colloids and Surfaces B: Biointerfaces 117:398–405. doi: 10.1016/j.colsurfb.2014.03.002

63. Pujana MA, Pérez-álvarez L, Carlos L, Iturbe C, Katime I (2013) Biodegradable chitosan nanogels crosslinked with genipin. Carbohydrate Polymers 94:836–842. doi: 10.1016/j.carbpol.2013.01.082

64. Moura M, Figueriredo M, Gil M (2007) Rheological study of genipin cross-linked chitosan hydrogels. Biomacromolecules 8:3823–3829.

65. Subramanian A, Lin H (2005) Crosslinked chitosan : Its physical properties and the effects of matrix stiffness on chondrocyte cell morphology and proliferation. doi:

10.1002/jbm.a.30489

66. Chou S, Lai J, Cho C, Lee C (2016) Colloids and Surfaces B : Biointerfaces Relationships between surface roughness / stiffness of chitosan coatings and fabrication of corneal keratocyte spheroids : Effect of degree of deacetylation. Colloids and Surfaces B: Biointerfaces 142:105–113. doi: 10.1016/j.colsurfb.2016.02.051

67. Fortier H, Variola F, Wang C, Zou S (2016) AFM force indentation analysis on leukemia cells. Anal Methods 8:4421–4431. doi: 10.1039/C6AY00131A

68. Kuo C-HR, Xian J, Brenton JD, Franze K, Sivaniah E (2012) Complex Stiffness Gradient Substrates for Studying Mechanotactic Cell Migration. Advanced Materials 24:6059–6064.

69. Wells RG (2008) The Role of Matrix Stiffness in Regulating Cell Behavior. Hepatology 47:1394–1400. doi: 10.1002/hep.22193

70. Ghimire H, Venkataramani M, Bian Z, Liu Y, Perera AGU (2017) ATR-FTIR spectral discrimination between normal and tumorous mouse models of lymphoma and melanoma from serum samples. Scientific Reports 7:1–9. doi: 10.1038/s41598-017-17027-4

71. Barth A (2007) Infrared spectroscopy of proteins. Biochimica et Biophysica Acta 1767:1073–1101. doi: 10.1016/j.bbabio.2007.06.004

72. Steeves AJ, Atwal A, Schock SC, Variola F (2016) Evaluation of the direct effects of poly(dopamine) on the in vitro response of human osteoblastic cells. Journal of Materials Chemistry B 4:3145–3156. doi: 10.1039/C5TB02510A

73. Gerstner W, Kreiter AK, Markram H, Herz AVM (1997) Neural codes : Firing rates and beyond. Proc Natl Acad Sci U S A 94:12740–12741.

74. Cunningham J., Gilja V, Ryu SI, Shenoy KV (2009) Methods for Estimating Neural Firing Rates, and Their Application to Brain-Machine Interfaces. Neural Networks2 22:1235–1246. doi: 10.1016/j.neunet.2009.02.004.Methods

75. Shadlen MN, Newsome WT (1998) The Variable Discharge of Cortical Neurons : Implications for Connectivity , Computation , and Information Coding. Journal of Neuroscience 18:3870–3896.

76. Markou A, D'Souza MS (2011) Neuronal Mechanisms Underlying Development of Nicotine Dependence: Implications for Novel Smoking-Cessation Treatments. Addiction Science & Clinical Practice 4–16.

77. Ugur S, Pekcan O (2006) Effects of Annealing on Morphology of Polymer/Polymer Blend; a Fluorescence Study. Journal of Applied Polymer Science 100:2104–2110.

78. Jin C, Olsen BC, Luber EJ, Buriak JM (2017) Nanopatterning via Solvent Vapor Annealing of Block Copolymer Thin Films. Chemistry of Materials 29:176–188.

79. Segalman RA (2005) Patterning with block copolymer thin films. 48:191–220. doi: 10.1016/j.mser.2004.12.003

80. Darling S (2007) Directing the self-assembly of block copolymers. 32:1152–1204. doi: 10.1016/j.progpolymsci.2007.05.004

81. Park WI, Kim Y, Jeong JW, Kim K, Yoo J, Hur YH, Kim JM, Thomas EL, Alexander-katz A, Jung YS (2013) Host-Guest Self-assembly in Block Copolymer Blends. Scientific Reports 3:1–10. doi: 10.1038/srep03190

82. Bywater S (1984) Block Polymers. Characterization and Use in Polymer Blends. Polymer Engineering and Science 24:104–111.

83. Butler HJ, Ashton L, Bird B, Cinque G, Curtis K, Dorney J, Esmonde-white K, Fullwood NJ, Gardner B, Martin-hirsch PL, Walsh MJ, Mcainsh MR, Stone N, Martin FL (2016) Using Raman spectroscopy to characterize biological materials. Nature Protocols 11:664–687. doi: 10.1038/nprot.2016.036

84. Bumbrah GS, Sharma RM (2016) Raman spectroscopy – Basic principle, instrumentation and selected applications for the characterization of drugs of abuse. Egyptian Journal of Forensic Sciences 6:209–215.

85. Hu B, Kong L-B, Kang L, Yan K, Zhang T, Li K, Luo Y-C (2017) Synthesis of a hierarchical nanoporous carbon material with controllable pore size and effective surface area for high-performance electrochemical capacitors. RSC Advances 7:14516–14527. doi: 10.1039/C7RA01151B

86. Huang Y-C, Huang C-C, Yi-You H, Chen K-S (2007) Preparation and Cytotoxicity of Poly(Methyl Methacrylate) Nanoparticles for Drug Encapsulation. Journal of Biomedical Materials Research 82A:842–851.

87. Mendes AN, Hubber I, Siqueira M, Barbosa GM, De Lima Moreira D, Holandino C, Pinto JC, Nele M (2012) Preparation and cytotoxicity of poly(methyl methacrylate) nanoparticles for drug encapsulation. In: Macromolecular Symposia. pp 34–40

88. León-Bermúdez AY, Salazar R (2008) Synthesis and characterization of the polystyrene - Asphaltene graft copolymer by FT-IR spectroscopy. CTyF - Ciencia, Tecnologia y Futuro 3:157–167.

89. Gershenbaum MR, Roisen FJ (1981) Applications of scanning electron microscopy in neuroscience research. Trends in Neurosciences 109–114.

90. Marcus M, Baranes K, Park M, Choi IS, Kang K (2017) Interactions of Neurons with Physical Environments. Advanced Healthcare Materials 6:1–19. doi: 10.1002/adhm.201700267

91. Song Y, Chen D, Zhao L (2017) Introduction: The Origin, Current Status, and Future of Microfluidics. Microfluidics: Fundamentals, Devices and Applications

92. Zander N, Beebe TJ (2014) Immobilized laminin concentration gradients on electrospun fiber scaffolds for controlled neurite outgrowth. Biointerphases 9:11003.

93. Romano NH, Lampe KJ, Xu H, Ferreira MM, Heilshorn SC (2015) Microfluidic gradients reveal enhanced neurite outgrowth but impaired guidance within 3D matrices with high integrin ligand densities. Small 11:722–730. doi: 10.1002/smll.201401574

94. Sundararaghavan HG, Monteiro GA, Firestein BL, Shreiber DI (2009) Neurite growth in 3D collagen gels with gradients of mechanical properties. Biotechnology and Bioengineering 102:632–643. doi: 10.1002/bit.22074

Appendices

Supplemental Figures

Table 5. Statistical analysis with ANOVA ($p<0.05$) for neuron adhesion on various surface coatings shown in Figure 10. 0 represents no significance, while 1 represents the two factors are statistically significant.

	Ch + PDA	**PDA**	**75:25 Ch:Collagen + PDA**	**Collagen**	**Laminin + PDL**	**Laminin + PDL + PDA**	**Matrigel**	**Matrigel + PDA**
Ch + PDA	-	0	1	0	0	0	0	1
PDA	0	-	1	1	0	1	1	1
Ch 75: Collagen 25 + PDA	1	1	-	0	1	0	0	0
Collagen	0	1	0	-	1	0	0	0
Laminin + PDL	0	0	1	1	-	1	1	1
Laminin + PDL + PDA	0	1	0	0	1	-	0	0
Matrigel	0	1	0	0	1	0	-	0
Matrigel + PDA	1	1	0	0	1	0	0	-

Table 6. Statistical analysis with ANOVA ($p<0.05$) for neurite outgrowth on various surface coatings shown in Figure 10. 0 represents no significance, while 1 represents the two factors are statistically significant.

	Ch + PDA	**PDA**	**75:25 Ch:Collagen + PDA**	**Collagen**	**Laminin + PDL**	**Laminin + PDL + PDA**	**Matrigel**	**Matrigel + PDA**
Ch + PDA	-	1	1	0	1	0	0	1
PDA	1	-	1	1		1	1	1
Ch 75: Collagen 25 + PDA	1	1	-	1	1	1	1	0
Collagen	0	1	1	-	1	0	0	1
Laminin + PDL	1	0	1	1	-	1	1	1
Laminin + PDL + PDA	0	1	1	0	1	-	0	1
Matrigel	0	1	1	0	1	0	-	1
Matrigel + PDA	1	1	0	1	1	1	1	-